All-in-one glycol chitosan nanoparticles for co-delivery of doxorubicin and anti-PD-L1 peptide in cancer immunotherapy

Sukyung Song [a,1], Man Kyu Shim [b,1], Suah Yang [b], Jaewan Lee [b,c], Wan Su Yun [b,c], Hanhee Cho [a], Yujeong Moon [b,d], Jin Young Min [e,f], Eun Hee Han [e], Hong Yeol Yoon [b], Kwangmeyung Kim [a,*]

[a] College of Pharmacy, Graduate School of Pharmaceutical Sciences, Ewha Womans University, Seoul, 03760, Republic of Korea
[b] Medicinal Materials Research Center, Biomedical Research Division, Korea Institute of Science and Technology (KIST), Seoul, 02792, Republic of Korea
[c] KU-KIST Graduate School of Converging Science and Technology, Korea University, Seoul, 02841, Republic of Korea
[d] Department of Bioengineering, Korea University, Seoul, 02841, Republic of Korea
[e] Research Center for Bioconvergence Analysis, Korea Basic Science Institute (KBSI), Cheongju, 28119, Republic of Korea
[f] Department of Toxicology, College of Pharmacy, Chungnam National University, Daejeon, 34134, Republic of Korea

ARTICLE INFO

ABSTRACT

Synergistic immunotherapy of immune checkpoint blockade (ICB) and immunogenic cell death (ICD) has shown remarkable therapeutic efficacy in various cancers. However, patients show low response rates and undesirable outcomes to these combination therapies owing to the recycling mechanism of programmed death-ligand 1 (PD-L1) and the systemic toxicity of ICD-inducing chemotherapeutic drugs. Herein, we propose all-in-one glycol chitosan nanoparticles (CNPs) that can deliver anti-PD-L1 peptide (PP) and doxorubicin (DOX) to targeted tumor tissues for a safe and more effective synergistic immunotherapy. The PP-CNPs, which are prepared by conjugating ᴅ-form PP (NYSKPTDRQYHF) to CNPs, form stable nanoparticles that promote multivalent binding with PD-L1 proteins on the targeted tumor cell surface, resulting in effective lysosomal PD-L1 degradation in contrast with anti-PD-L1 antibody, which induces recycling of endocytosed PD-L1. Consequently, PP-CNPs prevent subcellular PD-L1 recycling and eventually destruct immune escape mechanism in CT26 colon tumor-bearing mice. Moreover, the ICD inducer, DOX is loaded into PP-CNPs (DOX-PP-CNPs) for synergistic ICD and ICB therapy, inducing a large number of damage-associated molecular patterns (DAMPs) in targeted tumor tissues with minimal toxicity in normal tissues. When the DOX-PP-CNPs are intravenously injected into CT26 colon tumor-bearing mice, PP and DOX are efficiently delivered to the tumor tissues *via* nanoparticle-derived passive and active targeting, which eventually induce both lysosomal PD-L1 degradation and substantial ICD, resulting in a high rate of complete tumor regression (CR: 60%) by a strong antitumor immune response. Collectively, this study demonstrates the superior efficacy of synergistic immunotherapy using all-in-one nanoparticles to deliver PP and DOX to targeted tumor tissues.

1. Introduction

Among the cancer immunotherapy strategies that can initiate or enhance an antitumor immune response, immune checkpoint blockade (ICB) therapy *via* the monoclonal antibody (mAb) targeting programmed death-ligand 1 (PD-L1) has shown remarkable therapeutic efficacy in oncology patients [1,2]. In addition, the clinical outcomes of this antibody therapy have been significantly improved when combined with various immunogenic cell death (ICD)-inducing modalities,

including chemotherapy, radiotherapy, photodynamic therapy and photothermal therapy [3–6]. However, most patients respond poorly and show low response rates to these combination therapies. In particular, some tumors have been completely refractory to response with ICB [7,8]. This is due to the resistance mechanism by which PD-L1 endocytosed after conformational blockade with mAbs is actively recycled back to the cell surface through the recycling endosome, thereby preventing its degradation in the lysosome [9]. This recycling mechanism of endocytosed PD-L1 hinders to induce reliable and durable membrane

PD-L1 deficiency, thereby disrupting the signaling pathway of T cells and reducing ICB efficiency in cancer immunotherapy [10].

A subcellular trafficking strategy for lysosomal degradation of PD-L1 can be an important approach to improving the response rate and efficiency of ICB therapy by preventing the intracellular PD-L1 recycling mechanism. For instance, the depletion of PD-L1 regulator proteins, CMTM6 or trafficking protein particle complex subunit 4 (TRAPPC4), and the inhibition of PD-L1 palmitoylation using 2-bromopalmitate (2-BP) can cause lysosomal PD-L1 degradation by sorting endocytosed PD-L1 into lysosomes [11,12]. As a therapeutic approach, promoting multivalent binding of anti-PD-L1 antibodies or peptides with PD-L1 on the cell surface can efficiently transport PD-L1 to lysosomes to induce its lysosomal degradation [13]. It has been reported that multivalent binding complexes of ligands and receptors alter the endocytosis mechanism and subcellular trafficking, resulting in the internalization of their complexes into lysosomes [14]. Based on this multivalent binding mechanism of ligands and receptors, anti-PD-L1 peptide-conjugated 2-hydroxypropyl methacrylamide (HPMA) polymers promoted multivalent binding with PD-L1 on the cancer cell surface and induced lysosomal PD-L1 degradation to inhibit PD-L1 recycling to the cell surface compared with the monovalent binding mechanism of anti-PD-L1 mAbs [14]. In addition, nano-sized dendrimers modified with multiple anti-PD-L1 mAbs significantly improved the efficiency of ICB therapy *via* the PD-L1 multivalent binding mechanism [15]. Compared with anti-PD-L1 mAbs, these hyperbranched dendrimer-mediated PD-L1 multivalent binding substantially enhanced T-cell cytokine production by disrupting PD-1/PD-L1 immune escape and their resistance mechanisms in cancer cells. However, the exact mechanism through which multivalent binding promotes lysosomal PD-L1 degradation is not fully understood.

The efficacy of lysosomal PD-L1 degradation *via* multivalent binding can be determined by target accessibility, the number of ligands and expression levels of the target receptors on the cancer cell surface. However, a universal method in promoting multivalent binding of receptor-ligand complexes is still a major unmet clinical need [13]. As a promising approach, the nanoparticle system has high amenability for chemical modification to conjugate anti-PD-L1 ligands to induce multivalent binding to traffic PD-L1 proteins to subcellular lysosomes [16,17]. Furthermore, anti-PD-L1 ligand-modified nanoparticles can be used as a tumor-targeting delivery system for various immune modulators for synergistic immunotherapy owing to their high tumor accumulation by nanoparticle-derived passive and active targeting [18]. Therefore, discovering an all-in-one nanoparticle system incorporating ligands against PD-L1 with immune modulators, which can promote both lysosomal PD-L1 degradation by multivalent binding and elicit potent antitumor immunity, is a formidable challenge to improve the therapeutic efficacy of cancer immunotherapy. Recently, we studied the optimal density of anti-PD-L1 peptides on lipid nanoparticle surfaces to facilitate multivalent binding of PD-L1 on the cancer cell membrane *via* a clinically relevant liposomal formulation [19]. Interestingly, 10 mol% anti-PD-L1 peptide-incorporated liposomes effectively downregulated PD-L1 levels in cancer cells for 3 days by promoting multivalent binding-mediated lysosomal PD-L1 degradation, compared with a rapid PD-L1 recycling within 24 h of treatment with anti-PD-L1 mAb. Furthermore, loading an ICD inducer, doxorubicin (DOX), into the anti-PD-L1 peptide-modified liposomes successfully eradicated the targeted tumor tissues *via* synergistic immunotherapy of immunogenic chemotherapy and lysosomal PD-L1 degradation in colon tumor-bearing mice.

Herein, we propose a new all-in-one nanoparticle system consisting of anti-PD-L1 peptide-conjugated and DOX-loaded glycol chitosan nanoparticles (CNPs) to combine effective lysosomal PD-L1 degradation and ICD. The CNPs prepared with specific ratio of glycol chitosan and 5β-cholinic acid are excellent tumor-targeting nanoparticles that can be not only chemically modified with targeting ligands but also encapsulate different types of imaging agents, chemotherapeutic drugs, peptide

drugs, gene therapeutics and also immune modulators [20,21]. Furthermore, CNPs have shown outstanding advantages, such as efficient cellular uptake, high *in vivo* stability and good biocompatibility in cancer treatment. Notably, CNPs have shown a great tumor-targeting ability in many preclinical studies, thus they are most suitable nanoparticle systems for co-delivery of various ICD-inducing chemotherapeutic drugs with anti-PD-L1 peptide for cancer immunotherapy [22, 23]. To prepare a new all-in-one nanoparticle system, hydrophilic glycol chitosan polymer is chemically conjugated with hydrophobic 5β-cholanic acid. The resulting amphiphilic glycol chitosan-5β-cholanic acid conjugates form stable nanoparticle structures in aqueous conditions, resulting in CNPs. Then, anti-PD-L1 ᴅ-peptide (PP; NYSKPTDRQYHF) is conjugated to CNPs (PP-CNPs), followed by encapsulation of ICD-inducing chemotherapeutic drug, DOX, to yield DOX-PP-CNPs that can promote synergistic antitumor immune responses of ICB and ICD (Scheme 1a). When DOX-PP-CNPs are intravenously injected into tumor-bearing mice, they efficiently deliver PP and DOX to the targeted tumor tissues *via* both nanoparticle-derived passive and PD-L1 receptor-mediated active targeting mechanisms (Scheme 1b). Notably, the new all-in-one DOX-PP-CNPs promote multivalent binding with PD-L1 receptors on the tumor cell surface with aim to induce the lysosomal PD-L1 degradation that prevents PD-L1 recycling (Scheme 1c). Next, the receptor-mediated endocytosed DOX-PP-CNPs release DOX to induce potent ICD, resulting in dendritic cell (DC) maturation and T cell activation (Scheme 1d). Finally, PD-L1 multivalent binding of DOX-PP-CNPs significantly decrease an abundant PD-L1 expression induced following chemotherapy by promoting lysosomal PD-L1 degradation and preventing their recycling, thereby enhancing T cell-mediated antitumor immune responses to destroy the tumors. This study aims to investigate the effective lysosomal PD-L1 degradation by all-in-one nanoparticle-mediated PD-L1 multivalent binding *in vitro* and *in vivo*. Importantly, the exact mechanism of lysosomal PD-L1 degradation by multivalent binding of PP-CNPs with different amounts of anti-PD-L1 peptides (PP) on the nanoparticle surface is directly visualized in mGFP-tagged PD-L1-expressing tumor cells. Finally, a safe and more effective synergistic immunotherapy using DOX-PP-CNPs is assessed in the colon and metastatic lung tumor models.

2. Results and discussions

2.1. Preparation of anti-PD-L1 peptide-conjugated glycol chitosan nanoparticles (PP-CNPs)

First, we assessed whether PP-CNPs can induce lysosomal PD-L1 degradation *via* a multivalent binding mechanism. Briefly, CNPs were prepared by conjugating hydrophobic 5β-cholanic acid to hydrophilic glycol chitosan backbones (Fig. 1a and S1). The degree of substitution, defined as the number of 5β-cholanic acids per 100 residues of glycol chitosan, was determined to be 23% using the colloidal titration method and ¹H NMR [24]. Previously, these amphiphilic glycol chitosan-5β-cholanic acid conjugates were self-assembled into spherical nanoparticles (CNPs) with an average size of approximately 250 nm [25]. They exhibited prolonged *in vivo* circulation for passive tumor accumulation and could penetrate deep into the tumors owing to their great stability and deformability; hence, the tumor-targeting ability confirmed based on PET imaging was determined to be approximately 10% [21,26], which is the maximal value considering recent negative consequences of nanoparticles showing 1–2% of the total administered amount being accumulated in the tumor tissues [27]. In addition, the free amine groups in the CNPs were further modified with tumor-targeting antibodies and peptides for targeted tumor drug delivery [28]. Finally, hydrophobic chemotherapeutic drugs, such as DOX [29], paclitaxel [30], docetaxel [31], cisplatin [32], camptothecin [33], chlorin e6 [34] and protoporphyrin IX [35], can be efficiently loaded into the inner 5β-cholinic acid cores *via* hydrophobic interactions. Therefore, we expected that the CNPs would significantly improve the
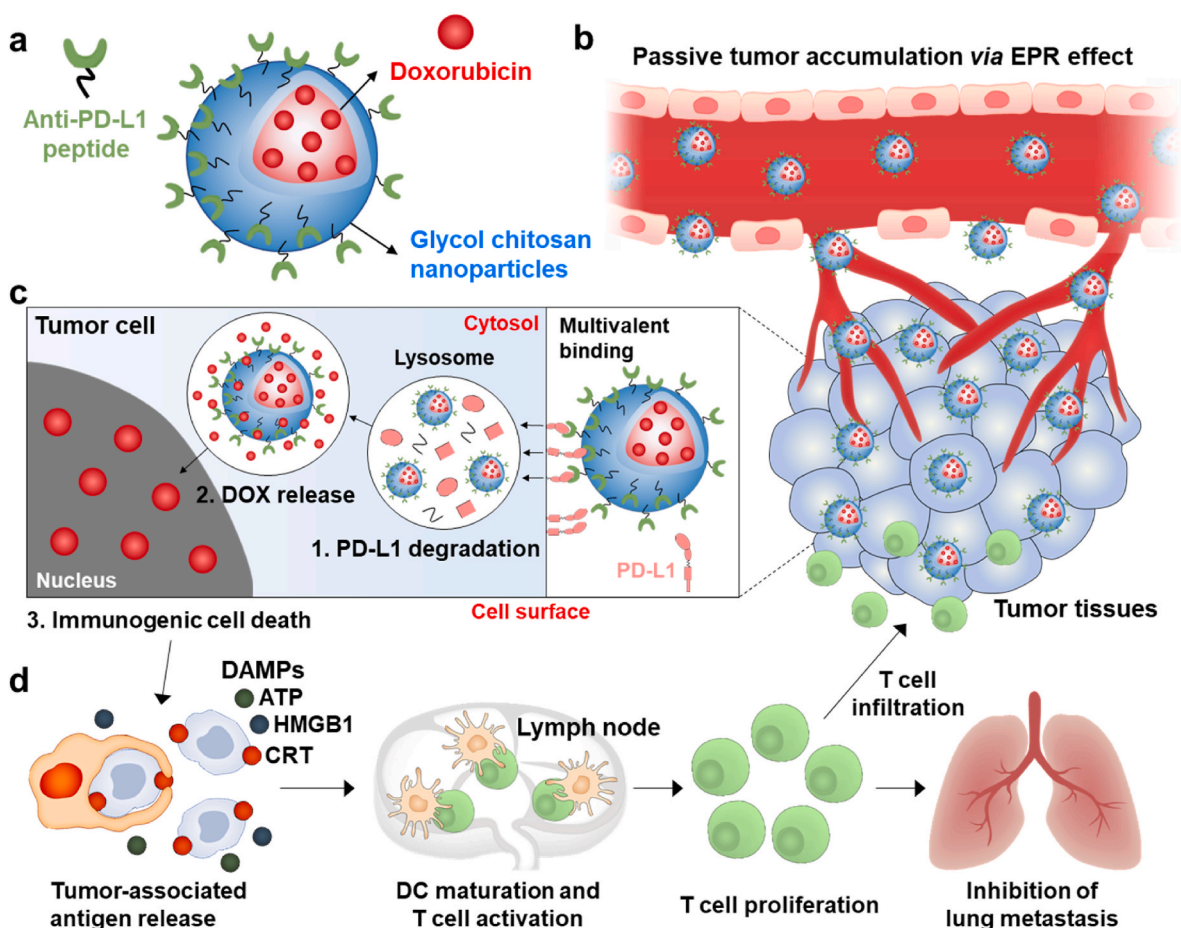
Scheme 1. Synergistic immunotherapy of PD-L1 degradation and ICD by DOX-PP-CNPs. (a) All-in-one nanoparticles, anti-PD-L1 peptide-conjugated and doxorubicin-loaded glycol chitosan nanoparticles (DOX-PP-CNP), are prepared for synergistic immunotherapy to combine PD-L1 degradation and ICD. **(b)** DOX-PP-CNPs are accumulated in targeted tumor tissues *via* both passive and active tumor targeting. **(c)** Then, DOX-PP-CNPs induce PD-L1 multivalent binding on the tumor cell surface, which internalize with aim to bias the intracellular trafficking of PD-L1 to lysosomes instead of recycling endosomes. **(d)** Endocytosed DOX-PP-CNPs release DOX to induce a potent ICD in the tumor cells, resulting in a large amount of DAMPs and tumor-associated antigens for DC maturation and T cell activation. In addition, PD-L1 multivalent binding of DOX-PP-CNPs significantly decrease a PD-L1 overexpression induced following chemotherapy by promoting lysosomal PD-L1 degradation and preventing their recycling. As a result, antitumor immune responses by synergistic immunotherapy of DOX-PP-CNPs based on PD-L1 degradation and ICD efficiently inhibit the progression and metastasis of tumors.

target accessibility of both the PP and DOX in tumor tissues.

To introduce the PP in the CNPs, bicyclo[6.1.0]nonyne (BCN) groups were conjugated to the amine groups of CNPs *via* an amide bond linkage, and the different amount of PPs that have azide (N$_3$) group in N-terminus was introduced *via* click chemistry reaction (Fig. 1a and S2). Recently, polymeric nanoparticles modified with anti-PD-L1 antibodies have been already studied [36,37]. However, since CNPs are modified under a harsh condition with organic solvent owing to its poor solubility in aqueous condition, the preparation of antibody-conjugated CNPs while maintaining three-dimensional structure of antibodies is very difficult. Therefore, we employed anti-PD-L1 peptide in developing the nanoparticle systems for multivalent binding-mediated PD-L1 degradation [38]. When the feeding amount of PP was increased from 7.5 to 25 wt% in the reaction solution, the amount of PP on CNPs was increased from 5.3 $\pm$ 0.75 (5 wt% anti-PD-L1 D-peptide conjugated CNPs; 5PP-CNPs), 10.9 $\pm$ 1.1 (10PP-CNPs) or 20.07 $\pm$ 1.88 wt% (20PP-CNPs), respectively (Fig. S4). Each PP-CNP showed a high PP conjugation efficiency (5 PP-CNPs: 70.67 $\pm$ 10%; 10PP-CNPs: 72.67 $\pm$ 7.33%; and 20PP-CNPs: 80.28 $\pm$ 7.52%) by copper-free click chemistry reaction that is capable of high yielding, simple to perform and create only by target products without additional catalysts [39–41]. The size and morphology of the PP-CNPs were not significantly changed after modification of CNPs with different amount of PPs, showing a spherical

structure of approximately 220–230 nm in diameter (Fig. 1b and c). In addition, no significant differences were observed in the zeta potential of the CNPs with different amounts of PP owing to the neutrally charged PP (Fig. S4). Next, the binding affinity of PP-CNPs to PD-L1 proteins was assessed *via* biolayer interferometry (BLI), wherein PP (0.067 μM), anti-PD-L1 mAb (PD-L1 Ab; 0.067 μM) and each PP-CNP with an equivalent concentration of PPs (0.067 μM) were used in the BLI analyses (Fig. 1d). As expected, the PD-L1 binding affinity of PP-CNPs gradually enhanced along to the increase of PP contents in CNPs from 5 to 20 wt%. In particular, the PD-L1 binding affinity of 10PP-CNPs was significantly higher than that of PP, PD-L1 Ab and 5 PP-CNPs, owing to the multivalent binding mechanism of PPs on the nanoparticle surface. However, 20PP-CNPs exhibited a PD-L1 binding affinity similar to that of 10PP-CNPs, indicating that PP-CNPs with 10 wt% PP are the optimal formulation to promote multivalent binding with PD-L1. These results are consistent with those of previous study that demonstrated the optimal density of 10 mol% anti-PD-L1 peptides on the liposome surface to facilitate PD-L1 multivalent binding for lysosomal degradation [19]. Thus, further studies were performed with 10PP-CNPs, which were denoted as PP-CNPs in next experiments. The PP-CNPs were highly stable in mouse serum without significant changes in particle size for 18 days, similar to the CNPs (Fig. 1e and S5). Their stable structure approximately 200 nm is suitable to accumulate within tumor tissues *via*
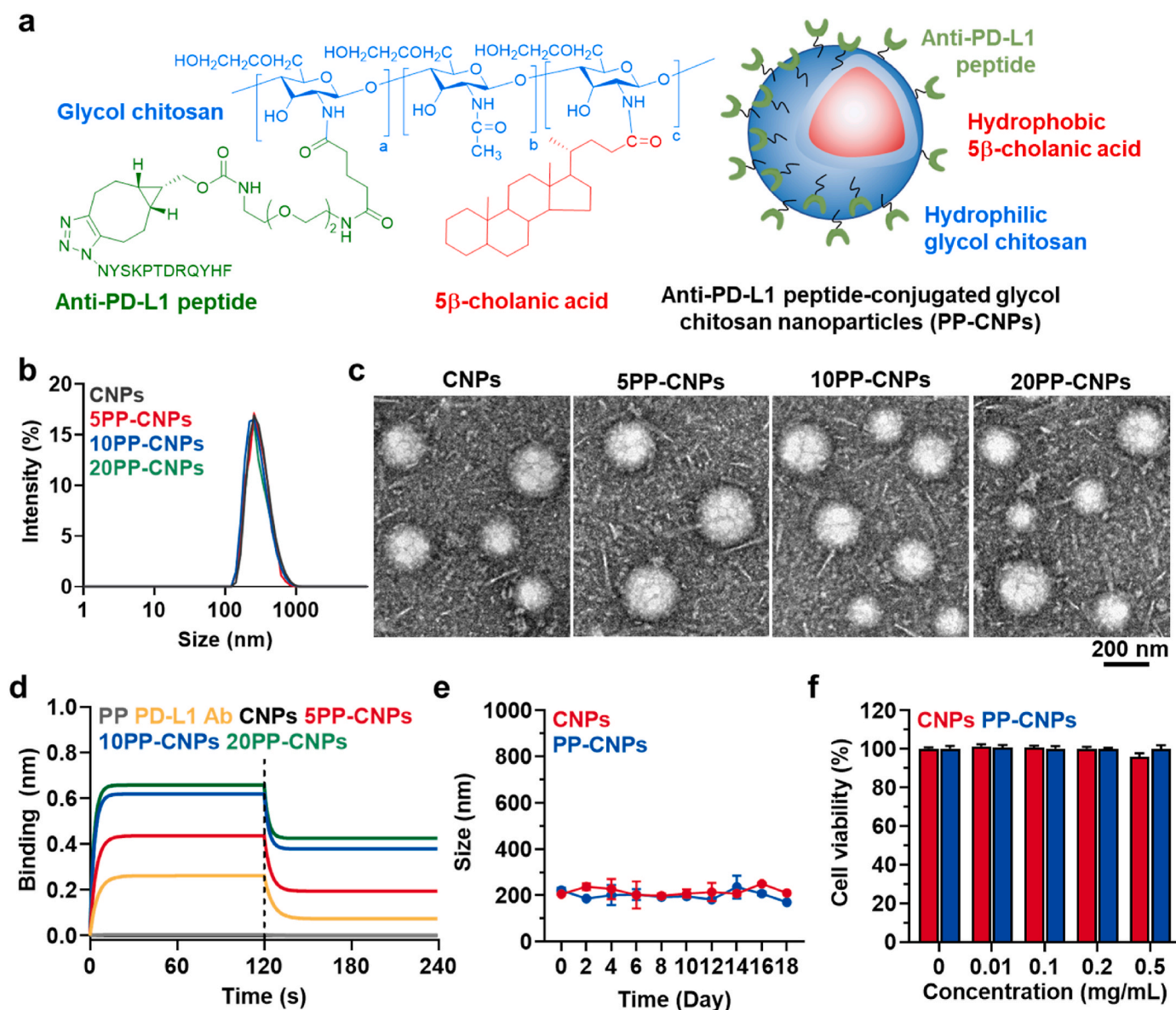
Fig. 1. Preparation and characterization of PP-CNPs. (a) Chemical structure of PP-CNPs. The glycol chitosan nanoparticles (CNPs) are prepared by conjugating 5β-cholanic acid to the glycol chitosan. Then, BCN groups are introduced in the amine group of glycol chitosan, and anti-PD-L1 peptide (PP; NYSKPTDRQYHF) is conjugated *via* the click chemistry reaction, resulting in PP-CNPs. **(b)** Size distribution of CNPs, 5PP-CNPs, 10PP-CNPs and 20PP-CNPs, as confirmed *via* DLS. **(c)** TEM images of CNPs, 5PP-CNPs, 10PP-CNPs and 20PP-CNPs. **(d)** Binding kinetics on PD-L1-derivatized biosensors of PD-L1 Ab, PP, CNPs or PP-CNPs containing different ratio of PP (5, 10 or 20%). The concentration of PP, PD-L1 Ab and PP in all the PP-CNPs was unified as 0.067 μM. **(e)** Stability of CNPs and PP-CNPs in the mouse serum for 18 days. **(f)** Cell viability of CT26 cells after treatment with CNPs or PP-CNPs for 48 h.

the EPR effect in different tumor-bearing mice [42,43]. To assess the biocompatibility of the nanoparticles, the viability of CT26 colon tumor cells and H9C2 normal cells was evaluated after treatment with CNPs or PP-CNPs for 48 h, showing no significant cytotoxicity (Fig. 1f and S6). These results indicate that the introduction of PP molecules did not affect the biocompatibility of the CNPs. Collectively, these characterization results demonstrate that the PP-CNPs with 10 wt% PP have suitable physicochemical characteristics to enhance target accessibility *via* the nanoparticle-derived EPR effect and efficiently promote PD-L1 multivalent binding for effective cancer immunotherapy.

2.2. Cellular binding and uptake of PP-CNPs in mGFP-tagged PD-L1-expressing tumor cells

PD-L1-mediated cellular binding and uptake of PP-CNPs were assessed in the PD-L1-overexpressing colon tumor cell line, CT26 [44].

To efficiently track the PP-CNPs in tumor cells, mGFP-CT26 cells that are prepared by transfection with lentiviral particles encoding mGFP-tagged PD-L1 were used for *in vitro* experiments. Homogeneous expression of mGFP-tagged PD-L1 (green color) in the cells was confirmed by flow cytometry and fluorescence imaging (Fig. S7). First, mGFP-CT26 cells were treated with PP-CNPs (0.067 μM based on PP) or anti-PD-L1 mAbs (PD-L1 Ab, 0.067 μM), labeled with the near-fluorescence dye Cy5.5, at 4 °C for 1 h and washed with PBS to remove unbound PP-CNPs or PD-L1 Ab to PD-L1. Then, the cells were further incubated at 37 °C for 24 h to investigate the cellular binding and uptake mechanism of PP-CNPs in comparison to PD-L1 Ab (Fig. 2). Both Cy5.5-labeled PP-CNPs and PD-L1 Ab (red color) were observed on the cell surface with strong co-localization (white arrow; orange color) to PD-L1 (green color) immediately after incubation. In the case of PD-L1 Ab, the orange color of the PD-L1 Ab/PD-L1 complexes was mainly observed on the cell membrane within 3 h post-incubation, and small amounts of these
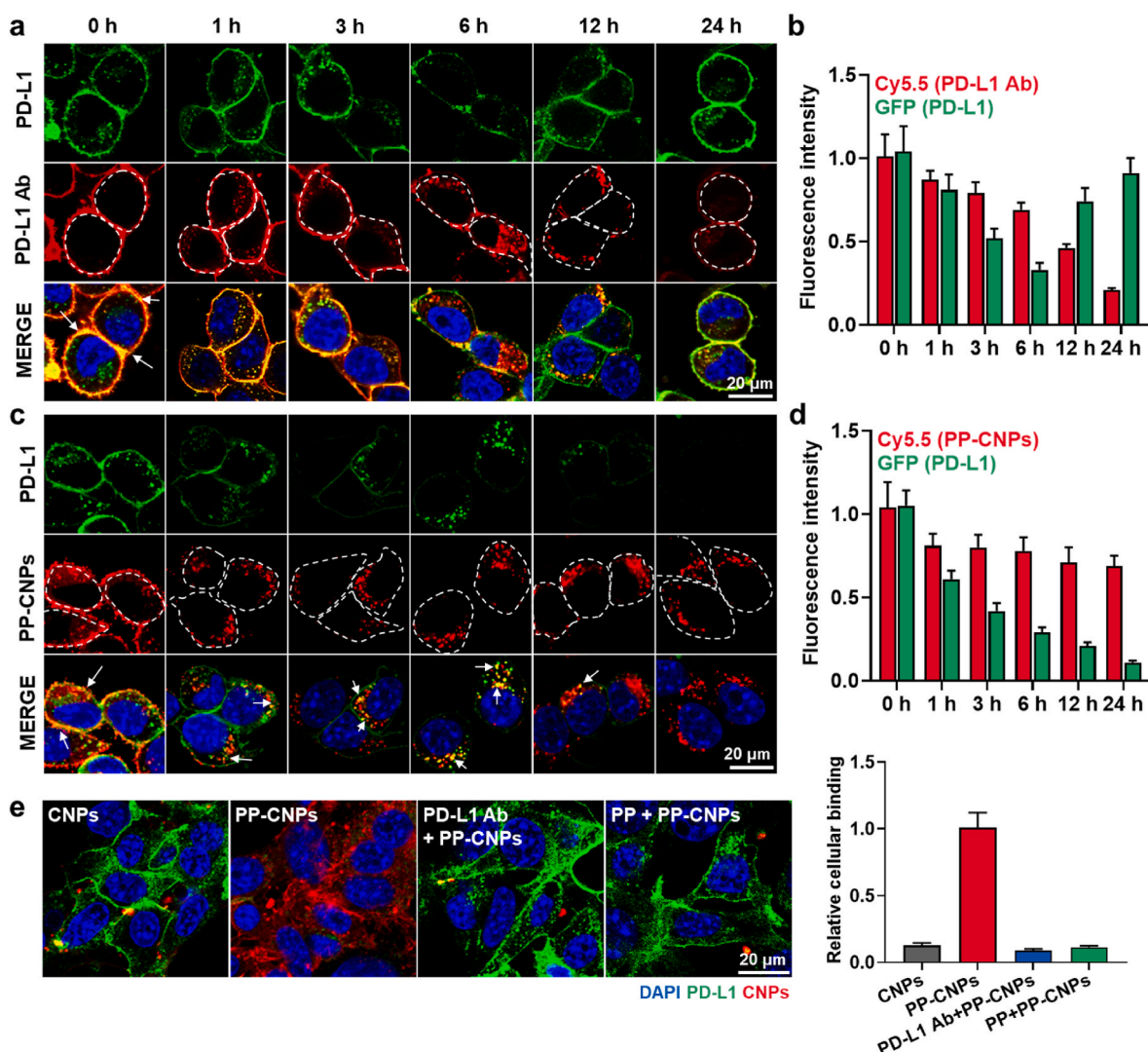
Fig. 2. Cellular binding and uptake of PP-CNPs. White dotted circles are the outer lines to show the morphology and boundary of cells. **(a)** The cellular binding and uptake of PD-L1 Ab in mGFP-tagged PD-L1-expressing CT26 (mGFP-CT26) cells. **(b)** Quantitative analysis for the amount of PD-L1 Ab in the mGFP-CT26 cells after treatment. **(c)** The cellular binding and uptake of PP-CNPs in mGFP-CT26 cells. **(d)** Quantitative analysis for the amount of PP-CNPs in the mGFP-CT26 cells after treatment. **(e)** The cellular binding and uptake of PP-CNPs after 1 h of treatment at 4 °C in the CT26 cells pre-treated with PD-L1 Ab or PP to block the PD-L1 on the cell surface.

complexes were internalized into the cells (Fig. 2a). Then, a large amount of PD-L1 Ab/PD-L1 complexes (orange color) was internalized into cells after 6 h of incubation, wherein only a small amount of PD-L1 (green color) was observed on the cell membrane. Importantly, the PD-L1 Ab/PD-L1 complexes were rapidly dissociated at 12 h post-incubation because they collapse more easily than the PD-L1/PD-1 axis [45]. This is also attributable to that the dissociation rate of PD-L1 Ab from PD-L1 is significantly accelerated in the acidic endosome [46]. In addition, PD-L1 Abs on the cell surface or cytoplasm were greatly reduced due to the extensive lysosomal degradation, thus PD-L1 regeneration was clearly observed on the cell membrane after 12 h of incubation. Quantitatively, PD-L1 in the cells was repopulated within 24 h of PD-L1 Ab treatment because most PD-L1 Ab (>90%) was removed from the cells at 12 h post-incubation (Fig. 2b). We assumed that this recycling mechanism of endocytosed PD-L1 significantly reduces the therapeutic efficacy of PD-L1 Abs in cancer immunotherapy [10].

In contrast, a large amount of PP-CNP/PD-L1 complex (orange color, white arrow) was rapidly internalized into the cytoplasm of tumor cells within 1 h post-incubation *via* nanoparticle-mediated endocytosis, with

approximately 90% of the PP-CNPs internalized into the cells (Fig. 2c). Then, most PP-CNP/PD-L1 complexes were sustainably localized in the cytoplasm for 24 h, indicating that their stable complex structure was maintained in the cytoplasm owing to the strong binding affinity attributed to the PD-L1 multivalent binding. These results indicate that multivalent binding of PP-CNPs with PD-L1 receptors can significantly enhance the internalization of PP-CNP/PD-L1 complexes in the cytoplasm compared with the monovalent binding of PD-L1 Ab [47]. Interestingly, over 80% of PP-CNPs was retained in the cytoplasm after 24 h of incubation, resulting in a significant decrease in PD-L1 expression levels to 11% compared with 0 h of incubation (Fig. 2d). As a control, CNPs in the absence of PP showed only a small cellular uptake compared with PP-CNPs at 4 °C for 1 h (Fig. S8). Finally, 1 h pre-treatment with anti-PD-L1 Ab or PP to competitively block PD-L1 on the cell surface significantly decreased the intrinsic cellular binding of PP-CNPs to 10% levels, which was similar to that of CNPs alone immediately after incubation (Fig. 2e). These *in vitro* results demonstrate the PD-L1-specific binding and uptake of PP-CNPs, and their complexes with PD-L1 show high stability due to multivalent binding, thereby internalizing rapidly into the tumor cells *via* PD-L1 receptor-mediated endocytosis [48].

2.3. Lysosomal PD-L1 degradation and T cell-mediated antitumor immune responses by PP-CNPs

Next, we evaluated whether PP-CNPs could induce lysosomal internalization of PD-L1 after multivalent binding-mediated endocytosis (Fig. 3a). When mGFP-CT26 cells treated with PP-CNPs (0.067 μM based on PP) were incubated at 37 °C, the internalized PP-CNPs (red color)/PD-L1 (green color) complexes migrated to the lysosomes (magenta color) over time in the cytoplasm (Fig. 3b and S9). Co-localization (white arrow; white color) of lysosomes (magenta color), PD-L1 (green color) and PP-CNPs (red color) was clearly observed in the cells, indicating that PP-CNPs entered the lysosomes while maintaining PD-L1 multivalent binding. Importantly, most PP-CNP/PD-L1 complexes were mainly localized in lysosomes at 12 h post-incubation, wherein PD-L1 proteins were irreversibly degraded in the cells. The percentage of PP-CNP/PD-L1 complexes observed in lysosomes gradually increased from 32.11% to 71.12% for 12 h of incubation (Fig. S9). In contrast, more than 90% of the PD-L1 Ab (red color)/PD-L1 (green color) complexes was located in the cell membrane, and 10% of complexes (orange color) was internalized into the cytoplasm after 3 h of incubation, wherein their co-localization (white arrow) with lysosomes (magenta color) was observed (Fig. 3c and S9). Then, internalization of PD-L1 Ab (red color) gradually increased in CT26 cells for 6 h post-incubation, but only 18% of PD-L1 Ab/PD-L1 complexes (white arrow) was localized in lysosomes. These results indicate that PD-L1 Ab/PD-L1 complexes are easily dissociated, and those dissociation rates of PD-L1 Ab from PD-L1 is significantly accelerated in the acidic endosome [40]. After 12 h of incubation, less than 5% of PD-L1 Ab/PD-L1 complexes were observed in the lysosomes in cells, with only a few co-localizations with lysosomes (Fig. S9). This is because subcellular trafficking of PD-L1 is prone to target recycling endosomes instead of lysosomes after binding to PD-L1 Ab [9]. These fluorescence imaging results confirm that PP-CNPs efficiently bias the subcellular trafficking of PD-L1 to the lysosomes instead of recycling endosomes *via* PD-L1 multivalent binding-mediated endocytosis.

Effective lysosomal PD-L1 degradation by nanoparticle-derived PD-L1 multivalent binding was evaluated in mGFP-CT26 cells after treatment with PP (0.067 μM), PD-L1 Ab (0.067 μM) or PP-CNPs (0.067 μM based on PP) at 37 °C for 72 h. In the case of the cells treated with PD-L1 Ab, PD-L1 (green color) was significantly decreased on the cell surface until 6 h after incubation, but it was rapidly recycled and repopulated from 12 h post-incubation (Fig. 3d). These results show that PD-L1 Ab-induced PD-L1 blockade results in PD-L1 recycling owing to its subcellular trafficking to target the recycling endosome and rapid repopulation after the dissociation of PD-L1 Ab from PD-L1. In contrast, PP-CNP-treated mGFP-CT26 cells showed durable PD-L1 degradation, wherein approximately 90% of PD-L1 disappeared from the cells after 24 h of treatment (Fig. S10a). The effective PD-L1 degradation by PP-CNPs is attributable to a multivalent binding-mediated endocytosis that detours PD-L1 to the lysosomes instead of recycling endosomes, as shown in Fig. 2 [14]. As a control, the patterns of PD-L1 expression in mGFP-CT26 cells treated with PP were similar to those treated with PD-L1 Ab, but their effects were significantly weak due to relatively low binding affinity (Fig. S10b). A significant decrease in the cellular abundance of PD-L1 by multivalent binding-mediated degradation was further confirmed by western blot analysis. After 48 h of treatment with PP (0.067 μM), PD-L1 Ab (0.067 μM) or PP-CNPs (0.067 μM based on PP), CT26 cells showed a significantly downregulated levels of PD-L1 to 12.2 ± 0.75% and 14.2 ± 1.3% after 48 h of treatment with PP-CNPs compared to the PP and PD-L1 Ab, respectively (Fig. 3e and S11).

Next, we assessed the effects of PP-CNPs to reinvigorate T cell activity *via* lysosomal PD-L1 degradation by exploiting co-culture assays. For these analyses, the CD8$^+$ T cells were isolated from the spleen and lymph nodes of BALB/c mice and activated with the anti-CD28 antibody on the culture plate coated with the anti-CD3 antibody. When the CT26 cells (1×10^5; red color) pre-treated with PP-CNPs (0.067 μM based on

PP) or PD-L1 antibody (0.067 μM) were co-cultured with CD8$^+$ T cells (5×10^5; green color) for 2 h at 37 °C, the number of CD8$^+$ T cells was significantly increased compared with those co-cultured with naive CT26 cells owing to T cell proliferation by target recognition (Fig. 3f). Notably, many CD8$^+$ T cells (white arrow) were strongly bound to PP-CNP-treated CT26 cells compared with naive or PD-L1 Ab-treated CT26 cells. This is attributable to the enhanced blockade of PD-1/PD-L1 interactions by efficient lysosomal PD-L1 degradation of PP-CNPs. Hence, co-culture with CT26 cells treated with PP-CNPs significantly upregulated CD8$^+$ T cell proliferation, wherein the percentages of proliferating T cells increased 6.01–6.23-fold and 1.67–1.92-fold compared with those co-cultured with naive or PD-L1 Ab-treated CT26 cells (Fig. 3g and h). In addition, IFN-γ secretion from activated T cells to the culture medium was also increased 12.43–12.83-fold and 2.21–2.4-fold compared with the control and PD-L1 Ab groups, respectively (Fig. 3i). As a result, tumor cell lysis was significantly elevated after treatment of CT26 cells with PP-CNPs compared with PD-L1 Ab when CT26 cells were co-cultured with CD8$^+$ T cells at a 1:5 (target to effector) ratio (Fig. 3j). Finally, higher expression of CD107a on CD8$^+$ T cells was clearly observed after co-culture with the CT26 cells treated with PP-CNPs than those treated with PD-L1 Ab, which indicates T cell degranulation by target recognition (Fig. 3k and S12). These *in vitro* experiments verify that PP-CNPs effectively promote durable lysosomal PD-L1 degradation *via* PD-L1 multivalent binding and subsequently block PD-1/PD-L1 interactions, thereby enhancing T cell-mediated antitumor immune responses.

2.4. In vivo tumor targeting and therapeutic efficacy of PP-CNPs in colon tumor models

The tumor targeting of PP-CNPs was assessed in colon tumor models, which were prepared *via* subcutaneous inoculation of 1×10^6 CT26 cells into the left flank of BALB/c mice. When the tumor volumes were approximately 200 mm^3, an equivalent dose (10 mg/kg) of PP-CNPs, CNPs, PD-L1 Ab or PP was intravenously injected into the mice. In terms of the amount of anti-PD-L1 ligands, ten times more PP compared to PP-CNPs were administered into mice owing to its poor tumor targeting and instability by extensive proteolysis. In addition, the maximum dose of PD-L1 Ab and PP-CNPs without any severe toxicity were intravenously injected into CT26 tumor-bearing mice. For non-invasive near-infrared fluorescence (NIRF) imaging, all samples were chemically labeled with the fluorescent dye Cy5.5. NIRF imaging showed poor tumor targeting and rapid clearance of Cy5.5-PP in CT26 tumor-bearing mice within 24 h by extensive proteolytic cleavage and short half-lives of the peptide structure (Fig. 4a) [49]. In contrast, Cy5.5-PD-L1 Ab-treated mice showed a slowly increased bright fluorescence signals in tumor tissues (black dotted circle) and reached its highest fluorescence intensities after 72 h of injection owing to large molecular weight and high affinity of PD-L1 Ab to PD-L1 receptors in targeted tumor tissues. As a positive control, Cy5.5-CNPs showed considerable tumor-targeting ability *via* nanoparticle-derived passive targeting, wherein the CNPs accumulated within the tumor tissues were sustainably retained for 72 h. CNPs have shown considerable tumor-targeting abilities in many preclinical studies owing to the EPR effect [31–33]. This substantial EPR effect of CNPs could be determined by ideal physicochemical properties, such as stability in serum, high deformability, prolonged circulation time in the blood, reduced reticuloendothelial system (RES) clearance, and fast cellular uptake into tumor cells [20]. In particular, Cy5.5-PP-CNPs highly accumulated in the tumor tissues within 6 h post-injection, and the bright NIRF signals of PP-CNPs in tumor tissues gradually increased up to 72 h, showing excellent tumor-targeting ability compared with PP, PD-L1 Ab and CNPs. Quantitatively, the tumor targeting efficiency of PP-CNPs was 20.07–20.88-fold, 5.92–6.21-fold and 2.23–2.7-fold higher than that of PP, PD-L1 Ab and CNPs, respectively (Fig. 4b). This suggests that tumor accumulation of PP-CNPs can be derived from both passive targeting
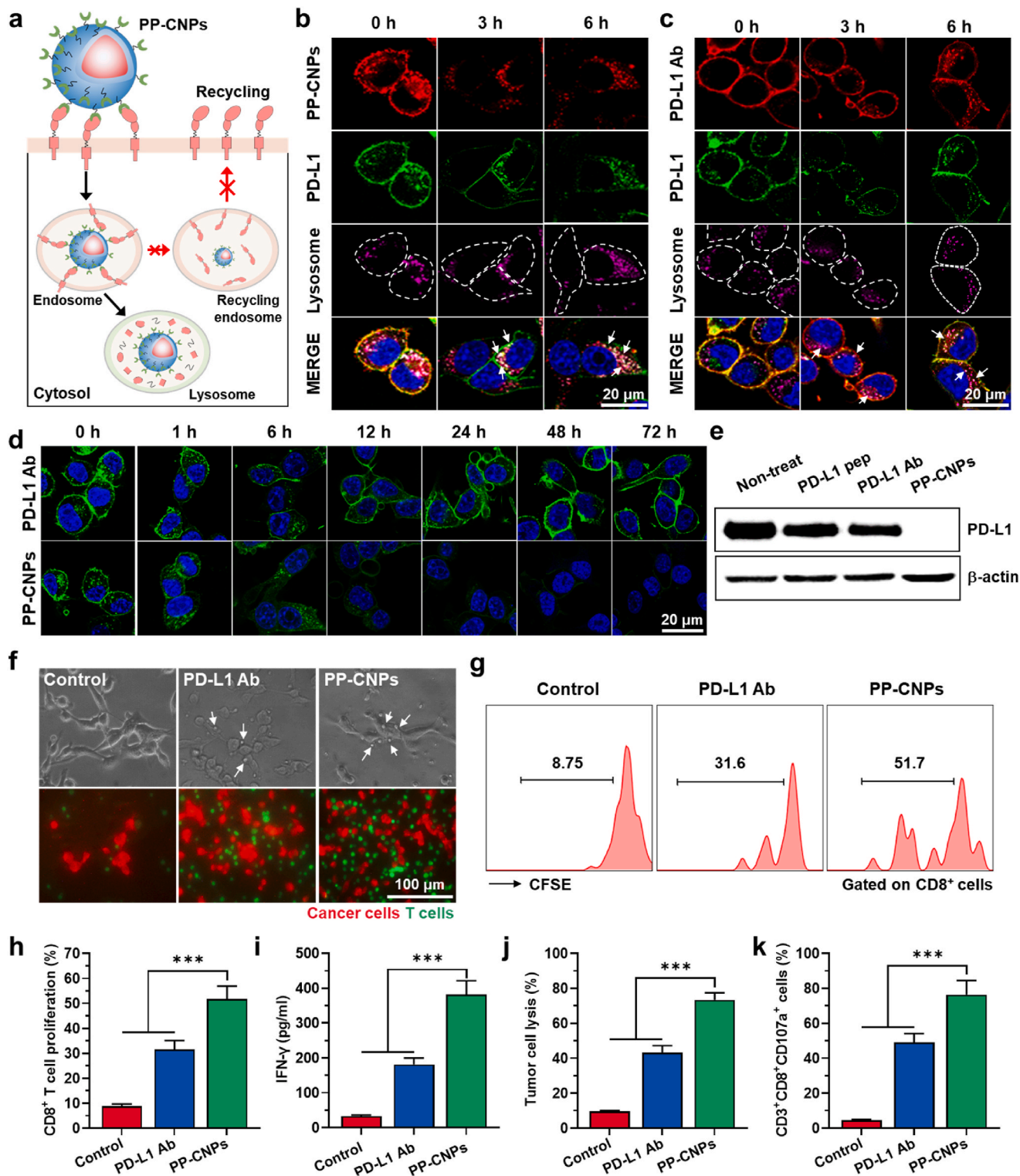
Fig. 3. Lysosomal PD-L1 degradation and T cell-mediated antitumor immune responses by PP-CNPs. **(a)** Schematic illustration showing multivalent binding-mediated lysosomal PD-L1 degradation by PP-CNPs. **(b, c)** Lysosomal localization of **(b)** PP-CNPs and **(c)** PD-L1 Ab after binding with PD-L1 in the mGFP-CT26 cells. The lysosomes were labeled with LAMP1-RFP fusion constructs. White dotted circles are the outer lines to show the morphology and boundary of cells. **(d)** Expression of PD-L1 in the mGFP-CT26 cells after treatment with PP-CNPs or PD-L1 Ab at 37 °C. **(e)** PD-L1 expression in mGFP-CT26 cells after treatment with PP-CNPs or PD-L1 Ab, as confirmed *via* western blot analysis. **(f)** Photographs and fluorescence images of CD8^{+} T cells co-cultured for 2 h with CT26 cells pre-treated with PP-CNPs or PD-L1 Ab. **(g)** T cell proliferation assays after 2 h of co-culture with CT26 cells pre-treated with PP-CNPs or PD-L1 Ab. **(h)** Quantitative analysis for the proliferating T cells after co-culture with CT26 cells pre-treated with PP-CNPs or PD-L1 Ab. **(i)** The amount of IFN-γ in the culture medium, **(j)** the levels of tumor cell lysis, and **(k)** CD107a exposure on T cells, after co-culture of CD8^{+} T cells with CT26 cells pre-treated with PP-CNPs or PD-L1 Ab. Significance was determined by Tukey−Kramer post-hoc test.
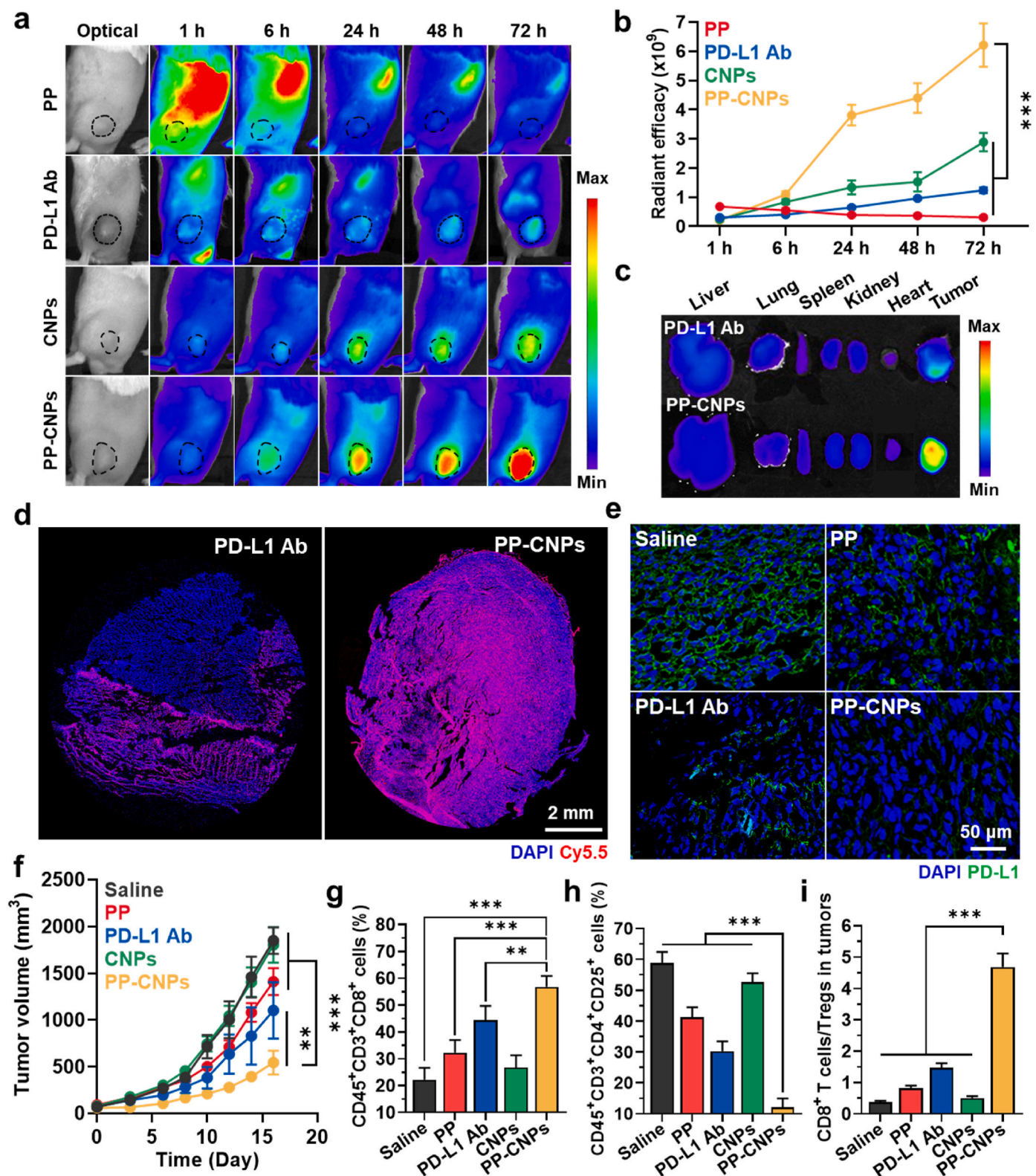
Fig. 4. *In vivo* **tumor targeting and therapeutic efficacy of PP-CNPs in colon tumor models. (a)** Noninvasive NIRF images of CT26 tumor-bearing mice treated with PP (anti-PD-L1 peptide), PD-L1 Ab, CNPs or PP-CNPs. **(b)** Quantitative analysis for the average fluorescence intensities in the tumor regions of NIRF images. **(c)** NIRF image of major organs and tumor tissues collected from mice treated with PD-L1 Ab or PP-CNPs after 72 h of injection. **(d)** Fluorescence images of tumor tissues from mice treated with PD-L1 Ab or PP-CNPs after 72 h of injection. **(e)** Tumor tissues stained with GFP fluorescent dye-conjugated anti-PD-L1 antibody after 72 h of treatment with PP, PD-L1 Ab, CNPs or PP-CNPs. **(f)** Tumor growth curves of CT26 tumor-bearing mice during treatment with PP, PD-L1 Ab, CNPs or PP-CNPs once every three days. **(g–i)** The population of **(g)** cytotoxic T cells ($CD45^+CD3^+CD8^+$) and **(h)** regulatory T cells ($CD45^+CD3^+CD4^+CD25^+$), and **(i)** ratio of cytotoxic T cells to regulatory T cells in the tumor tissues, after 10 days of treatment. Significance was determined by Tukey−Kramer post-hoc test.

and PD-L1-mediated active targeting mechanisms, which can lead to high target accessibility.

The *ex vivo* fluorescence imaging of major organs and tumors further confirmed a significantly high tumor accumulation of PP-CNPs after 72 h of injection, wherein the fluorescence intensity in tumor tissues was 18.31–18.77-fold, 5.31–5.99-fold and 1.71–1.79-fold higher than that of PP, PD-L1 Ab and CNPs, respectively (Fig. 4c and S13). In addition, PP-CNPs showed very low accumulation in normal organs, preventing non-specific drug delivery. Immunohistochemistry (IHC) showed a high accumulation of PP-CNPs (red color) in the whole area of the tumor tissues at 72 h post-injection, indicating that they could penetrate deep tumor tissues and remain in tumor tissues for 3 days (Fig. 4d and S14). In contrast, significantly less amounts of PP (5.52–5.77%) and PD-L1 Ab (18.32–20.06%) were observed in the extracted tumor tissues compared to PP-CNPs. As a positive control, CNPs showed considerable accumulation in targeted tumor tissues owing to their passive targeting ability. Based on these *in vivo* experiments, we confirmed that PP-CNPs, a new all-in-one nanoparticle for drug delivery, are highly accumulated in targeted tumor tissues *via* both passive and PD-L1-mediated active targeting. Notably, histological analyses also showed significantly lower PD-L1 expression (green color) in the tumor tissues from mice treated with PP-CNPs than in other treatment groups, thereby demonstrating effective *in vivo* PD-L1 degradation (Fig. 4e). In contrast, PP- or PD-L1 Ab-treated mice induced weak PD-L1 downregulations because of their poor tumor-targeting ability in CT26 tumor-bearing mice. As a control, tumor tissues from mice treated with CNPs showed PD-L1 expression levels that were comparable to those of the saline group. Effective *in vivo* PD-L1 degradation by multivalent binding was further investigated *via* western blot analysis (n = 3), wherein the levels of PD-L1 expression in tumor tissues were significantly downregulated to 26.7 ± 0.91% and 39.3 ± 1.07% after 72 h of treatment with PP-CNPs compared with PP and PD-L1 Ab, respectively (Fig. S15). In addition, the effects of multivalent binding-mediated lysosomal PD-L1 degradation of PP-CNPs were also observed in the tumor-associated immune cells. The population of PD-L1-positive DCs (CD11c$^+$PD-L1$^+$) and macrophages (F4/80$^+$PD-L1$^+$) within tumor tissues was significantly downregulated in PP-CNPs group, compared to other groups after 72 h of injection (Fig. S16). These results indicate that PP-CNPs efficiently promote the multivalent binding-mediated degradation of PD-L1 overexpressed on tumor tissue-associated DCs and macrophages that play an important role in immunosuppression [50]. Taken together, PP-CNPs efficiently accumulate within the tumor tissues *via* passive and active targeting for target access and promote effective *in vivo* PD-L1 degradation.

Next, the therapeutic efficacy and antitumor immune response of PP-CNPs were assessed in colon tumor models. The mice were randomly divided into five groups when the tumor volumes were approximately 60–80 mm^3; saline or 10 mg/kg of PP, PD-L1 Ab, CNPs or PP-CNPs were then intravenously injected into the mice once every 3 days. As expected, the mice treated with PP-CNPs (545.3 ± 127.8 mm^3) exhibited significantly delayed tumor growth on day 16 after treatment compared with saline (1850.51 ± 141.55 mm^3), PP (1411.61 ± 145.61 mm^3), PD-L1 Ab (1102.41 ± 301.51 mm^3) and CNPs (1803.88 ± 190.35 mm^3) groups (Fig. 4f). The low therapeutic efficacy of PD-L1 Ab and PP is due to their undesirable biodistribution, lower tumor-targeting ability and the recycling mechanism of PD-L1 proteins in targeted tumor cells [9]. To evaluate the antitumor immune responses to each treatment, the cytotoxic T cells (CD45$^+$CD3$^+$CD8$^+$) and regulatory T cells (Treg; CD3$^+$CD4$^+$CD25$^+$) in the tumor tissues were assessed on day 10 after treatment. As expected, the cytotoxic T cell proportions in the tumor tissues were 2.41–2.44-fold, 1.81–1.88-fold, 1.47–1.5-fold and 2.31–2.36-fold higher in the PP-CNPs group than in the saline, PD-L1 pep, PD-L1 Ab and CNPs groups, respectively (Fig. 4g and S17a). This is attributable to the effective PD-L1 degradation by PD-L1 multivalent binding of PP-CNPs, which enhances the target recognition and activity of T cells, resulting in an increase in tumor-infiltrating cytotoxic T cells.

In contrast, the proportion of Tregs in the tumor tissues was significantly lower in the PP-CNPs group than in the other groups (Fig. 4h and S17b). Consequently, tumors from mice treated with PP-CNPs recruited a large number of tumor-infiltrating cytotoxic T cells and excluded Tregs, resulting in an increased ratio of cytotoxic T cells to Tregs (Fig. 4i).

2.5. Preparation of all-in-one DOX-PP-CNPs for synergistic immunotherapy

Effective PD-L1 degradation by PD-L1 multivalent binding of PP-CNPs was clearly evaluated *in vitro* and *in vivo*. Thus, we hypothesized that loading DOX into PP-CNPs would induce potent synergistic immunotherapy to promote ICD and PD-L1 degradation (Fig. 5a). This new all-in-one nanoparticle system can overcome the fundamental problems of the most promising approach in the clinic, such as the severe off-target toxicity of anticancer drugs and anti-PD-L1 mAbs in normal tissues. ICD-inducing DOX was physically loaded into PP-CNPs using a simple dialysis method, wherein 10.2 ± 0.07 wt% of DOX with 51 ± 0.35% loading efficiency was successfully loaded into the hydrophobic cores of the nanoparticles. The DOX-PP-CNPs showed a spherical nanoparticle structure with an average size of 208.3–231.7 nm similar to that of PP-CNPs in aqueous conditions (Fig. 5b and S18). In addition, DOX-PP-CNPs maintained their nanoparticle size in mouse serum for 10 days (Fig. 5c and S19). In contrast to free DOX rapidly released out from cellulose membranes (MWCO: 100 kDa) within 6 h of incubation, DOX-PP-CNPs and DOX-CNPs showed similar delayed drug release profiles with approximately 80% of DOX released from both nanoparticles within 72 h of incubation (Fig. 5d). This is because free DOX molecules are released very slowly from the hydrophobic inner cores of CNPs [51]. As a result, the cytotoxicity of DOX-PP-CNPs and DOX-CNPs was similar in CT26 cells after 48 h of treatment, which was slightly reduced compared with free DOX (Fig. 5e). The PP-CNPs showed a significantly high cellular uptake at 4 °C after removal with 1 h post-incubation compared to CNPs owing to PD-L1 binding mechanism as shown in Fig. 2c and S8. However, the amount of both nanoparticles in CT26 cells after 48 h of treatment at 37 °C was nearly similar because CNPs also have intrinsically high cellular uptake *via* micropinocytosis, clathrin- and caveolae-mediated endocytosis (Fig. S20) [52]. Therefore, the cytotoxicity by intracellular DOX delivery of PP-CNPs and CNPs was nearly similar owing to their comparable cellular uptake and delayed drug release profile.

Next, ICD in CT26 cells induced by DOX release from DOX-PP-CNPs was evaluated by measuring DAMPs, such as calreticulin (CRT) expression on the cell surface and extracellular release of high mobility group box 1 (HMGB1) and adenosine triphosphate (ATP). The CRT in the cells was analyzed by fluorescence imaging after 48 h of treatment. The CRT expression levels on the CT26 cell surface were similar when they were treated with equivalent DOX concentrations (1 μM) of free DOX (6.01 ± 0.55-folds compared to naive cells), DOX-CNPs (6.67 ± 0.72-folds) or DOX-PP-CNPs (7.17 ± 0.79-folds; Fig. 5f). In addition, CT26 cells released similar levels of HMGB1 and ATP after treatment with free DOX (3.15 ± 0.41-folds and 3.78 ± 0.37-folds of HMGB1 and ATP compared to naive cells, respectively), DOX-CNPs (2.77 ± 0.28-folds and 3.54 ± 0.14-folds) or DOX-PP-CNPs (3.33 ± 0.51-folds and 3.48 ± 0.14-folds) for 48 h (Fig. 5g). As a control, treatment with PP-CNPs in absence of DOX did not induce an ICD in CT26 cells, showing a similar expression of CRT, HMGB1 and ATP compared to naive cells. We further performed co-culture assays to demonstrate that DAMPs expression in tumor cells by DOX-PP-CNPs result in DC maturation to promote tumor-associated antigen presentation for cytotoxic T cell activation. For these studies, CT26 cells were treated with equivalent DOX concentrations (1 μM) of free DOX, DOX-CNPs and DOX-PP-CNPs for 48 h, followed by an additional incubation of the cell culture medium containing DAMPs released from dying cells with lymphocytes from BALB/c mice for 2 h (Fig. 5h). Importantly, the proportion of mature DCs (CD11c$^+$CD40$^+$CD86$^+$) in the lymphocytes was similar in
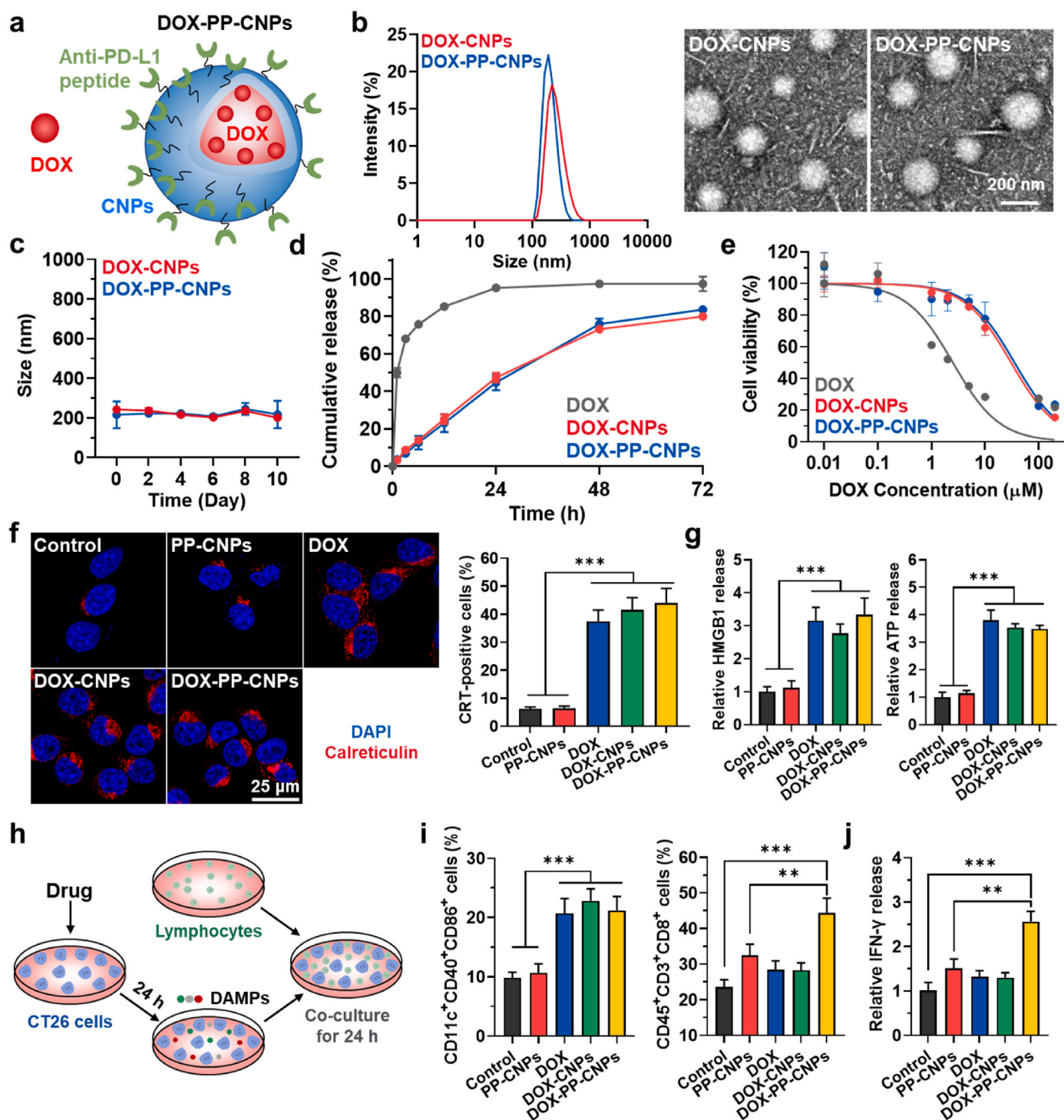
Fig. 5. Preparation of all-in-one DOX-PP-CNPs for synergistic immunotherapy. (a) Schematic illustration showing structure of all-in-one nanoparticles, DOX-PP-CNPs. **(b)** Size distribution and morphology of DOX-CNPs and DOX-PP-CNPs, as confirmed *via* DLS and TEM, respectively. **(c)** Stability of DOX-CNPs and DOX-PP-CNPs in the mouse serum for 10 days. **(d)** DOX release profiles of DOX-CNPs and DOX-PP-CNPs. Free DOX, DOX-CNPs and DOX-PP-CNPs were loaded into inner space of cellulose membranes (MWCO: 100 kDa) in PBS (pH 7.4) containing 0.1% Tween 80. Then, the amount of free DOX leaked to outer membrane was measured using UV–vis spectrometer at 480 nm wavelength. **(e)** The viability of CT26 cells treated with free DOX, DOX-CNPs or DOX-PP-CNPs for 48 h. **(f)** Fluorescence images and flow cytometry results (n = 3) of CT26 cells stained with anti-CRT antibody after treatment with PP-CNPs or an equivalent DOX concentration (1 μM) of free DOX, DOX-CNPs or DOX-PP-CNPs for 48 h. **(g)** The amount of HMGB1 and ATP released from CT26 cells treated with PP-CNPs or an equivalent DOX concentration (1 μM) of free DOX, DOX-CNPs or DOX-PP-CNPs for 48 h. **(h)** Schematic illustration to explain the protocol of co-culture assays. **(i)** Percentage of mature DCs (CD11c$^+$CD40$^+$CD86$^+$) and cytotoxic T cells (CD45$^+$CD3$^+$CD8$^+$) in lymphocytes after co-culture with culture medium containing DAMPs released from CT26 cells treated with PP-CNPs, free DOX, DOX-CNPs or DOX-PP-CNPs for 48 h. **(j)** Relative amount of IFN-γ in the culture medium after co-culture of lymphocytes with CT26 cells treated with PP-CNPs, free DOX, DOX-CNPs or DOX-PP-CNPs for 48 h. Significance was determined by Tukey–Kramer post-hoc test.

the free DOX, DOX-CNPs and DOX-PP-CNPs groups, whereas that of cytotoxic T cells (CD45$^+$CD3$^+$CD8$^+$) was significantly higher in the DOX-PP-CNPs group (Fig. 5i and S21). This indicates that the effects of DOX-PP-CNPs in promoting DC maturation by inducing DAMPs in tumor cells were similar to those of free DOX and DOX-CNPs, but the proliferation of cytotoxic T cells was significantly upregulated owing to their increased target recognition by multivalent binding-mediated PD-L1 degradation. Accordingly, IFN-γ released from T cells into the co-culture medium was also elevated due to the high activity of cytotoxic T cells after co-culture with CT26 cells treated with DOX-PP-CNPs compared with other treatments (Fig. 5j). As a control, there are no significant changes in DC maturation, T cell proliferation and IFN-γ release from T cells after lymphocytes were co-cultured with CT26 cells treated with PP-CNPs.

2.6. Effective synergistic immunotherapy by DOX-PP-CNPs in CT26 tumor-bearing mice

The *in vivo* enhanced therapeutic efficacy and antitumor immune responses by synergistic immunotherapy of DOX-PP-CNPs were evaluated in CT26 tumor-bearing mice. The mice were randomly divided into five groups: (i) saline, (ii) free DOX (1 mg/kg), (iii) DOX-CNPs (1 mg/kg based on DOX content), (iv) DOX-CNPs plus PD-L1 Ab (10 mg/kg), and (v) DOX-PP-CNPs (1 mg/kg based on DOX content). Each drug was intravenously injected into the mice once every 3 days, and PD-L1 Ab was simultaneously administered with DOX-CNPs *via* intravenous injection. As expected, the tumor growth of mice was significantly inhibited after 10 days of treatment with DOX-PP-CNPs (124.6 ± 63.4 mm^3) compared with saline (1860.36 ± 381.55 mm^3), free DOX (1066.95 ± 89.61 mm^3), DOX-CNPs (405.98 ± 19.96 mm^3) and DOX-CNPs plus PD-L1 Ab (206.99 ± 84.5 mm^3), which is attributable to the synergistic effect of multivalent binding-mediated PD-L1
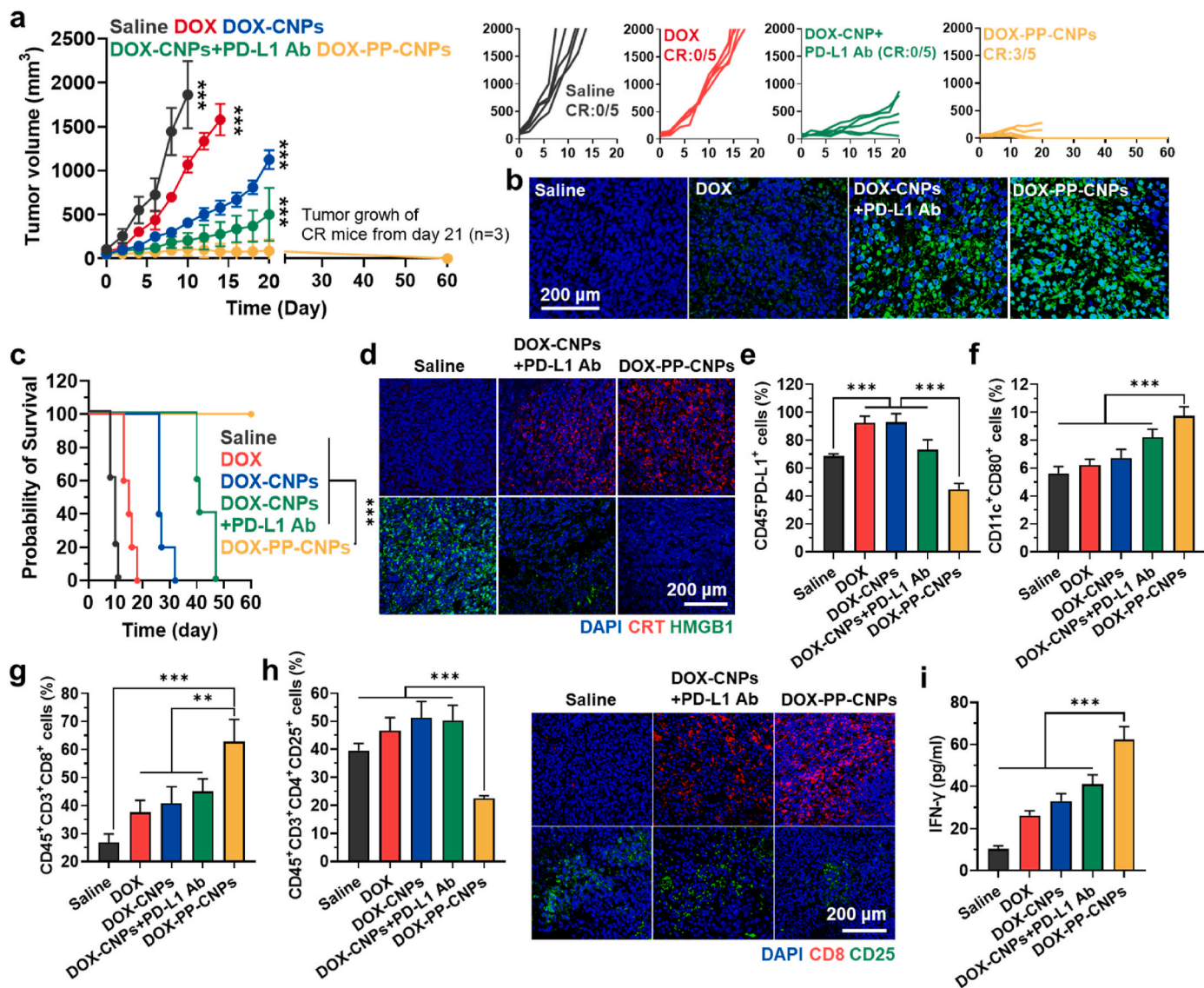

Fig. 6. Effective synergistic immunotherapy by DOX-PP-CNPs in CT26 tumor-bearing mice. (a) Tumor growth curves of CT26 tumor-bearing mice during treatment with free DOX, DOX-CNPs, DOX-CNPs plus PD-L1 Ab or DOX-PP-CNPs once every three days. **(b)** Tumor tissues stained with TUNEL after 10 days of treatment. **(c)** Mice survival during treatment. **(d)** Tumor tissues stained with anti-CRT or anti-HMGB1 antibodies after 10 days of treatment. **(e)** The population of PD-L1-positive tumor cells (CD45$^-$PD-L1$^+$) in the tumor tissues after 10 days of treatment. The population of **(f)** mature DCs (CD11c$^+$CD80$^+$) and **(g)** cytotoxic T cells (CD45$^+$CD3$^+$CD8$^+$) in the tumor tissues after 10 days of treatment. **(h)** The population of regulatory T cells (CD45$^+$CD3$^+$CD4$^+$CD25$^+$) in the tumor tissues after 10 days of treatment. Right panel show the tumor tissues stained with anti-CD25 antibody. **(i)** The amount of IFN-γ in the tumor supernatants after 10 days of treatment. Significance was determined by Tukey–Kramer post-hoc or log-rang (c) tests.

degradation and the potent DOX-mediated ICD (Fig. 6a and S22a). Notably, a high rate of complete tumor regression (CR: 60%) was observed in mice treated with DOX-PP-CNPs compared to that in the other groups; tumor growth of three mice that experienced complete tumor regression among the five mice in DOX-PP-CNPs was observed for 60 days, and other two mice were sacrificed on day 20 after treatment

for analysis of immune responses within the tumor tissues. The tumor tissues stained with TUNEL or H&E revealed considerably elevated apoptosis with structural abnormalities in the mice treated with DOX-PP-CNPs than in other treatment groups (Fig. 6b, S22b and S22c). As a result, the median survival of mice treated with saline, free DOX, DOX-CNPs or DOX-CNPs plus PD-L1 Ab was determined to be 10, 15, 26 and
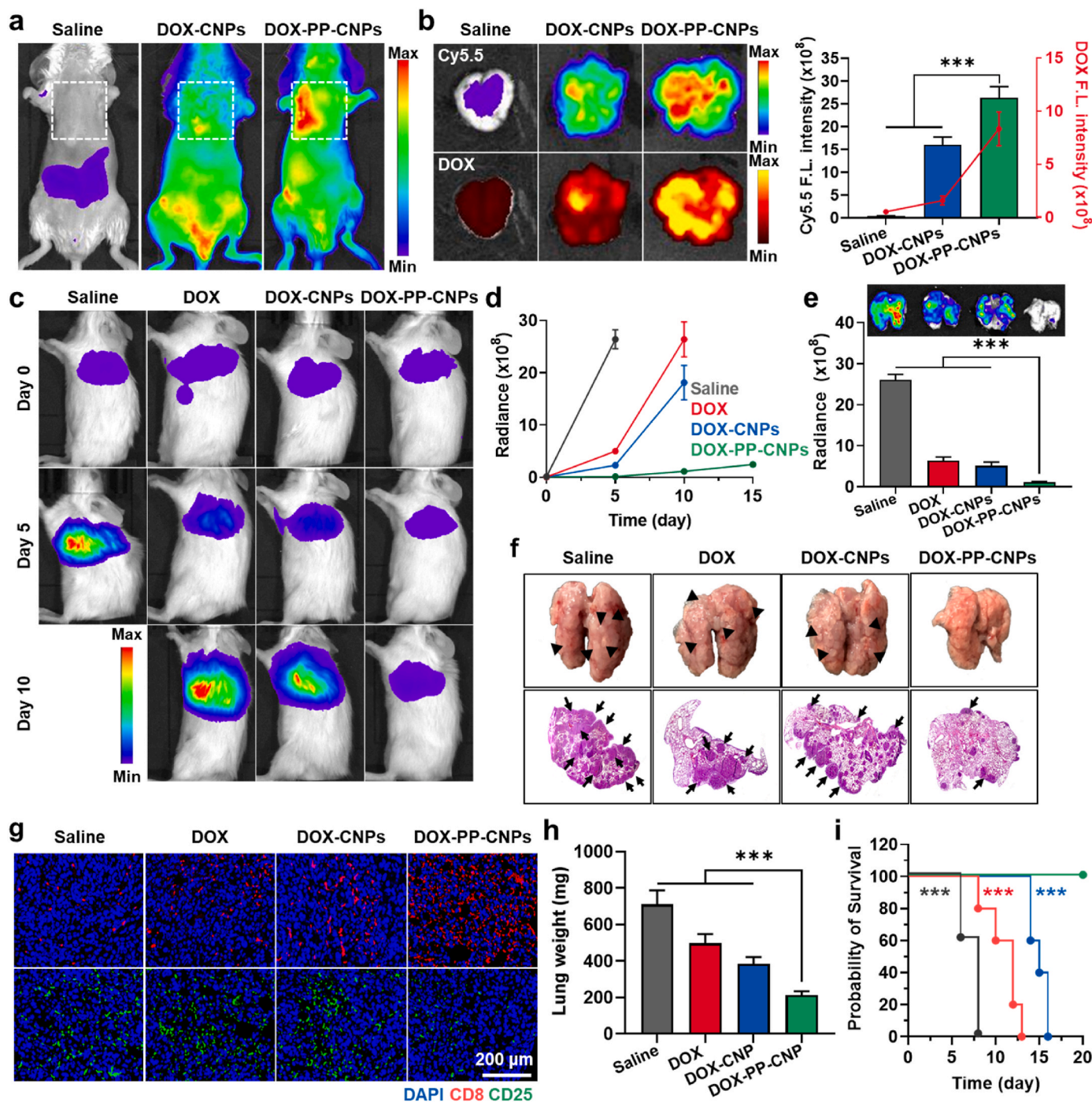

Fig. 7. Metastatic tumor inhibition by synergistic immunotherapy of DOX-PP-CNPs. (a) NIRF images of metastatic tumor models treated with DOX-CNPs or PP-DOX-CNPs for 72 h. **(b)** NIRF images of pulmonary tumor tissues of metastatic tumor models treated with DOX-CNPs or PP-DOX-CNPs for 72 h. Right panel show the quantitative analysis for fluorescence intensities of DOX-CNPs or PP-DOX-CNPs in the pulmonary tumor tissues. **(c)** Metastatic tumor growth monitored by bioluminescence imaging during treatment with free DOX, DOX-CNPs or DOX-PP-CNPs once every three days. **(d)** The average bioluminescence flux in the metastatic tumor region in the mice. **(e)** *Ex vivo* bioluminescence imaging and the average bioluminescence flux in pulmonary tumor tissues after 5 days of treatment. **(f)** Analysis of pulmonary tumor metastasis after 5 days of treatment. The metastatic tumor nodules were observed by photographing and staining with H&E. **(g)** Pulmonary tumor tissues stained with anti-CD8 or anti-CD25 antibodies after 5 days of treatment. **(h)** Weight of lung tissues collected from metastatic tumor models after 5 days of treatment. **(i)** Mice survival during treatment (n = 5). Significance was determined by Tukey–Kramer post-hoc (b, e and h) or log-rank (i) tests.

40 days, respectively, and the mice died due to tumor progression (Fig. 6c). In contrast, mice treated with DOX-PP-CNPs survived for over 60 days with significantly suppressed tumor growth.

To analyze antitumor immune responses, tumor tissues were collected from mice to assess the DAMP expression and the proportion of tumor-infiltrating lymphocytes on day 10 after treatment. First, tumor tissues from mice treated with DOX-PP-CNPs showed significantly upregulated CRT expression (red color) with reduced HMGB1 (green color) as a result of extracellular release compared to the other groups (Fig. 6d and S23). These high DAMP expressions are attributed to potent ICD by effective DOX delivery based on passive and active targeting of DOX-PP-CNPs. Treatment with free DOX or DOX-CNPs resulted in the negative feedback of abundant PD-L1 expression, whereas tumor tissues from the DOX-CNPs plus PD-L1 Ab group showed decreased PD-L1 expression compared with the free DOX and DOX-CNPs groups (Fig. 6e). Most importantly, DOX-PP-CNPs significantly downregulated chemotherapy-induced PD-L1 overexpression by promoting multivalent binding-mediated PD-L1 degradation, wherein the tumor tissues revealed a lower PD-L1 expression compared with all other groups. As a result, the proportion of mature DCs and cytotoxic T cells in the tumor tissues was 1.8–1.88-fold and 2.31–2.4-fold, 1.53–1.61-fold and 1.61–1.68-fold, 1.43–1.49-fold and 1.52–1.55-fold, and 1.21–1.24-fold and 1.35–1.38-fold higher in mice treated with DOX-PP-CNPs than in those treated with saline, free DOX, DOX-CNPs and DOX-CNPs plus PD-L1 Ab, respectively (Fig. 6f and g). These results indicate that DOX-PP-CNPs elicit a potent ICD in tumor cells to promote DC maturation for cross presentation of tumor-associated antigens to T cells owing to a synergistic DOX delivery and multivalent binding-mediated PD-L1 degradation. In contrast, the proportion of Tregs in the tumor tissues was significantly downregulated in the DOX-PP-CNPs groups, resulting in an increase in the ratio of cytotoxic T cells to Tregs (Fig. 6h and S24). Finally, the high activity of cytotoxic T cells in the tumor tissues in the DOX-PP-CNPs group was confirmed by measuring the elevated quantities of IFN-γ released from activated T cells in the tumor microenvironment (Fig. 6i). These findings demonstrate the superior antitumor efficacy of synergistic immunotherapy owing to ICD and multivalent binding-mediated PD-L1 degradation, *via* the CNPs.

2.7. Metastatic tumor inhibition by synergistic immunotherapy of DOX-PP-CNPs

Finally, we investigated whether the synergistic immunotherapy of DOX-PP-CNPs could effectively prevent tumor metastasis. Pulmonary metastatic tumor models were prepared by intravenous injection of 1×10^6 luciferase-expressing CT26 cells into BALB/c mice. First, the high metastatic tumor targeting of PP-DOX-CNPs was evaluated by NIRF imaging, wherein a strong Cy5.5-fluorescent signals from the periphery of the lungs were observed after 72 h of injection (Fig. 7a). Notably, *ex vivo* NIRF imaging of lung tissues also showed significantly higher fluorescence signals of Cy5.5 (Ex/Em:633/670, 1.66–1.73-fold) and DOX (Ex/Em:530/590, 3.88–4.01-fold) in the PP-DOX-CNPs group than in the DOX-CNPs group (Fig. 7b). These results indicate that DOX-PP-CNPs efficiently delivered DOX to metastatic tumor tissues *via* passive and active tumor targeting. To assess antitumor efficacy in the metastatic tumor models, saline or equivalent doses (1 mg/kg based on DOX content) of free DOX, DOX-CNPs or DOX-PP-CNPs were intravenously injected into the mice once every 3 days. The antitumor efficacy of each treatment was monitored using noninvasive bioluminescence imaging (Fig. 7c and S25). As the control, saline-treated mice showed strong bioluminescence signals on day 5, indicating rapid metastatic tumor growth. Mice treated with free DOX or DOX-CNPs showed significantly suppressed metastatic tumor growth compared with saline group after 5 days of treatment. However, treatment with free DOX and DOX-CNPs resulted in significant progression of metastatic tumors on day 10 because their efficacy was insufficient to treat highly aggressive metastatic tumors. In contrast, DOX-PP-CNPs effectively inhibited metastatic

tumor growth for 15 days, wherein the bioluminescence intensity in the mice treated with DOX-PP-CNPs was greatly decreased to 0.5–0.52%, 2.6–2.71% and 5.62–5.78% compared to those treated with saline, free DOX and DOX-CNPs on day 5, respectively (Fig. 7d). *Ex vivo* imaging further confirmed that metastatic tumor growth in the lung tissues of mice treated with DOX-PP-CNPs was significantly inhibited than other treatments on day 5 (Fig. 7e). In addition, we also observed significantly reduced metastatic tumor nodules in the lung tissues of the DOX-PP-CNPs group than in the other groups after 5 days of treatment; besides, lung tissues stained with H&E showed superior effects of DOX-PP-CNPs on inhibiting metastatic tumor growth, indicating a reduced metastatic tumor region (black arrow; Fig. 7f). Finally, pulmonary tumor tissues in the mice treated with DOX-PP-CNPs exhibited significantly upregulated cytotoxic T cells (CD8; red color) with reduced Tregs (CD25; green color), confirming potent synergistic immunotherapy of PD-L1 degradation and ICD to prevent tumor metastasis (Fig. 7g). As a result, DOX-PP-CNPs considerably reduced the weight of pulmonary tumor tissues (213.2 ± 20.18 mg) compared with saline (709.5 ± 77.31 mg), free DOX (496.9 ± 50.21 mg) and DOX-CNPs (383.7 ± 38.11 mg), thereby prolonging the survival of metastatic tumor models (Fig. 7h and i). These findings demonstrate that DOX-PP-CNPs effectively inhibit metastatic tumor growth *via* synergistic immunotherapy of PD-L1 degradation and ICD.

2.8. Toxicity study of DOX-PP-CNPs

The safety of DOX-PP-CNP treatment was assessed in BALB/c mice, which were treated with (i) saline, (ii) free DOX (1 mg/kg), (iii) DOX-CNPs (1 mg/kg based on DOX content), (iv) DOX-CNPs plus PD-L1 Ab (10 mg/kg), or (v) DOX-PP-CNPs (1 mg/kg based on DOX content) once every 3 days. The mice were treated as same protocol as described in Fig. 6. First, free DOX-treated mice showed significant body weight loss due to severe systemic toxicity, whereas no significant body weight changes were observed in the mice treated with DOX-PP-CNPs or DOX-CNPs compared with those treated with saline (Fig. 8a). Furthermore, hematological and histological analyses were performed after 10 days of treatment. The blood analyses showed severe cardiac, hepatic and renal toxicities in free DOX-treated mice, as confirmed by significant changes in the hematological parameters, including alanine transaminase (ALT), aspartate aminotransferase (AST), creatinine kinase (CK) and blood urea nitrogen (BUN; Fig. 8b and S26). In contrast, these parameters in the DOX-PP-CNPs and DOX-CNPs groups were in normal range and similar to in the saline group. The major organ tissues stained with H&E exhibited extensive damaged areas (indicated as black arrows) in the free DOX group, but only negligible structural abnormalities were observed in major organs of mice treated with DOX-PP-CNPs or DOX-CNPs (Fig. 8c). These toxicity studies indicate that DOX-PP-CNPs efficiently minimize systemic toxicity *via* high tumor targeting with low non-specific delivery of DOX.

2.9. Conclusion

In this study, we proposed a new all-in-one nanoparticle system of DOX-PP-CNPs for synergistic immunotherapy combining lysosomal PD-L1 degradation and ICD. DOX-PP-CNPs efficiently accumulated within the tumor tissues *via* passive and active targeting. More importantly, they promoted PD-L1 multivalent binding on the tumor cell surface, detouring PD-L1 into the lysosomes instead of recycling endosomes. The DOX-PP-CNPs internalized in the cells released DOX, which induced potent ICD that led to DC maturation and T cell activation by high DAMP expression. Meanwhile, PD-L1 multivalent binding of DOX-PP-CNPs significantly decreased chemotherapy-induced PD-L1 overexpression by promoting lysosomal PD-L1 degradation and preventing their recycling. As a result, synergistic immunotherapy of PD-L1 degradation and ICD disrupted the immune escape mechanism in tumor cells and increased the activity of T cells by target recognition to enhance
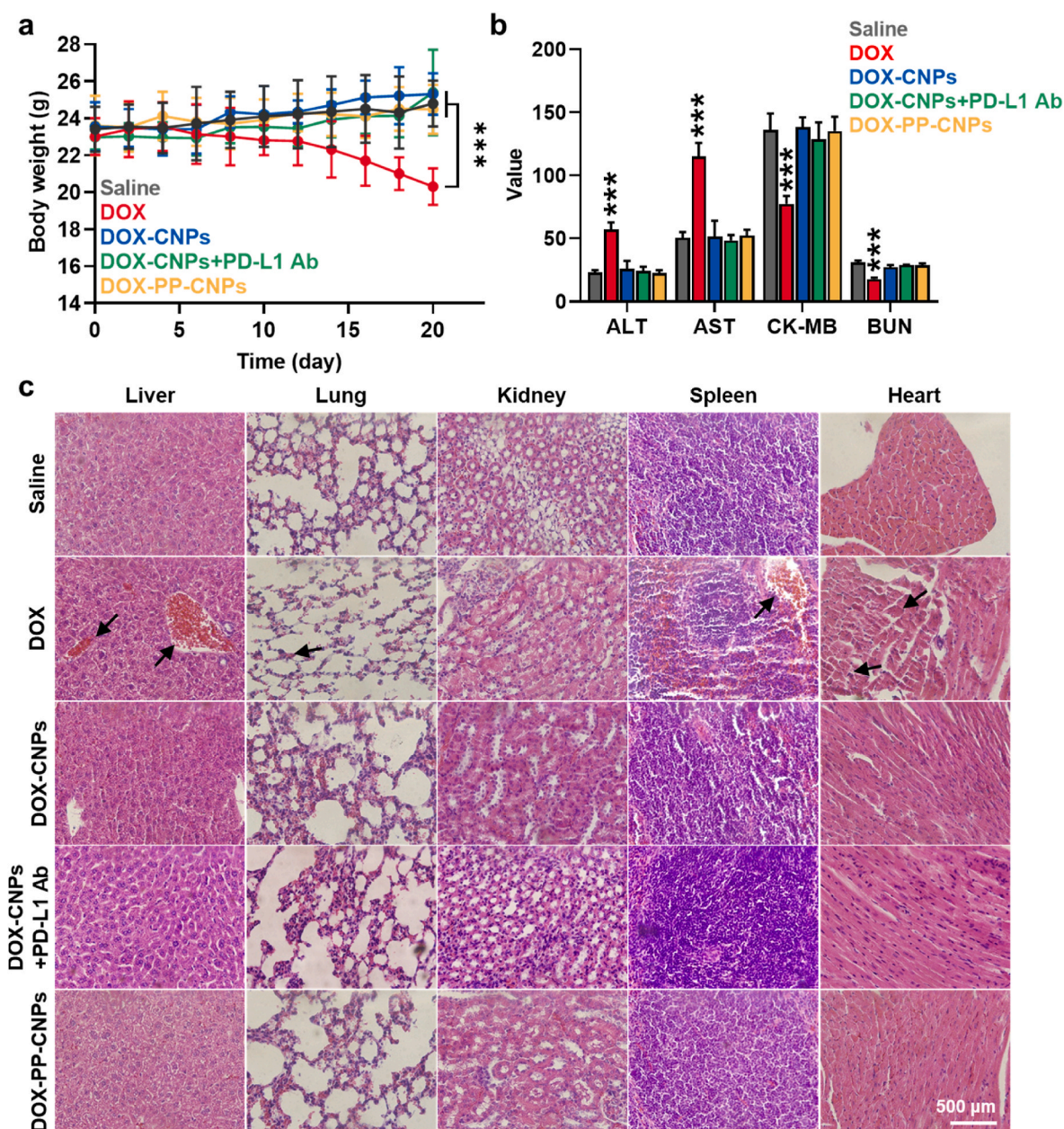
Fig. 8. Toxicity study of DOX-PP-CNPs. (a) Body weight changes of mice during treatment with free DOX, DOX-CNPs, DOX-CNPs plus PD-L1 Ab or DOX-PP-CNPs once every three days. **(b)** Hematological parameters of mice treated with free DOX, DOX-CNPs, DOX-CNPs plus PD-L1 Ab or DOX-PP-CNPs for 10 days. **(c)** Major organ tissues stained with H&E of mice treated with free DOX, DOX-CNPs, DOX-CNPs plus PD-L1 Ab or DOX-PP-CNPs for 10 days. Black arrows indicate structural abnormalities. Significance was determined by Tukey–Kramer post-hoc test.

antitumor immune responses. Finally, we evaluated the superior effects of DOX-PP-CNPs in inhibiting tumor growth in colon tumors and metastatic tumor models *via* a strong antitumor immune response. Collectively, our findings suggest that rationally designed CNPs promote synergistic immunotherapy of PD-L1 degradation and ICD providing a new route for effective ICB therapy.

3. Materials and methods

3.1. Reagents

Glycol chitosan (Mw = 250 kDa; degree of deacetylation = 82.7%), 5β-cholanic acid, doxorubicin hydrochloride, 1-ethyl-3-(3-dimethylaminopropyl)-carbodiimide hydrochloride (EDC) and N-hydroxysuccinimide (NHS) were purchased from Sigma Aldrich (St. Louis, MO,

USA). Bicylco[6.1.0]nonyne N-hydroxysuccinimide ester II (BCN–NHS) was purchased from Berry & Associates (Dexter, MI, USA). Flamma 648 NHS ester was purchased from BioActs (Incheon, Republic of Korea). Tem grid (Carbon Film 200 Mesh copper) was purchased from Electron Microscopy Sciences (Hatfield, PA, USA). N-terminal azidoacetylated PD-L1 binding peptide *Asn-Tyr-Ser-Lys-Pro-Thr-Asp-Arg-Gln-Tyr-His-Phe* (Azidoacetyl-NYSKPTDRQYHF) was purchased from Peptron (Daejeon, Republic of Korea). Cell counting kit-8 (CCK-8) was purchased from Vitascientific (Beltsville, MD, USA). Anti-mouse calreticulin (cat# ab196159) was purchased from Abcam (Hanam, Republic of Korea). Cy5.5-conjugated PD-L1 antibody (Cy5.5-PD-L1 Ab) was purchased from BioLegend (San Diego, CA, USA). Fluorescent dye-conjugated antibodies against mouse CD45.2 (cat# 109828), mouse CD3 (cat# 100218), mouse CD8a (cat# 100712), mouse CD4 (cat# 100412), mouse CD25 (cat# 126404), mouse PD-L1 (cat# 124312), mouse CD11c

(cat# 117310), mouse F4/80 (cat# 123116) and red blood cell lysis buffer (cat# 420301) were purchased from BioLegend (San Diego, CA, USA). IFN-γ Quantikine ELISA Kit (cat# SMIF00) and CD8$^+$ T cell column kit (cat# MCD8C-1000) were purchased from R&D system (Minneapolis, MN, USA). Tumor dissociation kit (cat# 130-096-730) and T cell Activation/Expansion Kit (cat# 130-093-627) were purchased from Miltenyi Biotechnoloy (Bergisch Gladbach, North Rhine-Westphalia, Germany). Human Tagged ORF Clone Lentiviral Particle (mGFP-tagged PD-L1) was purchased from ORIGENE (Rockville, MD, USA). CT26 (mouse colon cancer cells) was purchased from American Type Culture Collection (ATCC; Manassas, VA, USA). Fetal bovine serum (FBS), streptomycin, penicillin and RPMI 1640 medium were purchased from WELGENE Inc. (Daegu, Republic of Korea).

3.2. Preparation and characterization of glycol chitosan nanoparticles

First, glycol chitosan nanoparticles (CNPs) were prepared *via* chemical conjugation of hydrophobic 5β-cholanic acid to the primary amine groups of glycol chitosan (GC). Briefly, 5β-cholanic acid (300 mg, 800 μmol), NHS (144 mg, 1.2 mmol), EDC (240 mg, 1.2 mmol) and GC (1 g, 2 μmol) were dissolved in methanol/distilled water mixture (1:1 v/v, 100 ml). The resulting solution was stirred at 37 °C for 12 h, followed by dialysis for 2 days in methanol/distilled water mixture (1:3 v/v) using a cellulose membrane (Molecular weight cut off (MWCO): 12,000–14,000). Then, the solution was further dialyzed for 2 days in distilled water and lyophilized to yield 5β-cholanic acid-glycol chitosan conjugates. The number of β-cholanic acid per one GC was measured by a colloidal titration method and ^{1}H NMR, wherein the final conjugates had approximately 220 molecules of 5β-cholanic acids per GC.

For the conjugation of anti-PD-L1 peptide (NYSKPTDRQYHF), BCN groups were additionally introduced in CNPs. Briefly, BCN–NHS (20 mg, 38 μmol) was dissolved in 1 ml of DMSO and added dropwise to the CNPs (200 mg) in DMSO/distilled water mixture (1:9 v/v, 20 ml). The reaction buffer was stirred at 37 °C for 48 h, dialyzed against distilled water using a cellulose membrane (Molecular weight cut off 12,000–14,000) for 2 days, and lyophilized to obtain BCN-CNPs as a white powder. Then, anti-PD-L1 peptide was conjugated to BCN-CNPs *via* click chemistry reaction. The anti-PD-L1 peptide (20 mg, 12 μmol) and BCN-CNPs (200 mg) were dissolved in 20 ml of DMSO. The reaction buffer was stirred at 37 °C for 12 h, dialyzed against distilled water using a cellulose membrane (MWCO: 12,000–14,000) for 2 days to remove the unreacted peptides, lyophilized to yield anti-PD-L1 peptide-conjugated glycol chitosan nanoparticles (PP-CNPs). The successful chemical conjugation of CNPs with PP was analyzed using 400 MHz ^{1}H NMR (DD2 FT NMR, Agilent Technologies, USA) after dissolving in DMSO-d_6 (Fig. S3). The glycol chitosan peaks in PP-CNPs are shown at 3.13–4.20 ppm and PP peaks in PP-CNPs are observed in 6.60–7.80 ppm which is related to benzene structure of PP molecules. On the other hands, CNPs have no peaks at 6.60–7.80 ppm, due to the lack of benzene structure of PP molecules. The concentration of anti-PD-L1 peptide in the PP-CNPs was determined *via* the BCA assay. For fluorescent labeling, PP-CNPs (301 kDa; 220 mg, 0.73 μmol) and Cy5.5-NHS (2 mg, 1.7 μmol) were dissolved in 80 ml of anhydrous DMSO. The blue solution was stirred for 1 day at room temperature and dialyzed against distilled water using a cellulose membrane (MWCO: 100 kDa) for 2 days, followed by lyophilization to obtain as powder of Cy5.5-labeled PP-CNPs.

To prepare anti-PD-L1 peptide-conjugated and doxorubicin (DOX)-loaded glycol chitosan nanoparticles (DOX-PP-CNPs), DOX was dissolved in tetrahydrofuran (THF) and added dropwise into the PP-CNP solution (200 mg/10 ml in DMSO). Then, the organic solvent was removed using the rotary evaporator to obtain the deposition of a thin film at the glass vial wall, followed by freeze-dry for 4 h to remove remaining organic solvent. The film was hydrated and dispersed in distilled water with sonication. Finally, the solution was passed through 0.45 μm syringe filter membrane to remove unloaded DOX. The DOX loading content and efficiency of DOX-CNPs and DOX-PP-CNPs were

determined using the UV–vis spectrometer at 480 nm wavelength. *In vitro* DOX release profiles of DOX-CNPs and DOX-PP-CNPs were assessed in 37 °C PBS containing 0.1% of Tween 80. Briefly, an equivalent DOX concentration (1 μM) of DOX-CNPs and DOX-PP-CNPs was dispersed in PBS (pH 7.4). Each solution was loaded into the dialysis membranes (MWCO: 100 kDa) and shaken at 37 °C under 100 rpm in a water bath. At the pre-determined time points, the amount of DOX released to outer membranes was quantified by using UV–vis spectrometer at 480 nm wavelength.

After preparation of CNPs, PP-CNPs, DOX-CNPs, DOX-PP-CNPs, their size distribution and morphology in saline (1 mg/ml) were confirmed using dynamic light scattering (DLS; Zetasizer Nano ZS, Malvern Instruments, UK) and transmission electron microscope (TEM; CM-200, Philips, USA), respectively. To verify PD-L1 multivalent binding of PP-CNPs, biolayer interferometry (BLI) were performed on a BLItz system. Briefly, 50 μg/ml of recombinant PD-L1 was immobilized on a Protein A biosensor (ForteBio, Menlo Park, California, USA). The biosensors were washed with kinetics buffer two times and reacted with anti-PD-L1 antibody, anti-PD-L1 peptide (NYSKPTDRQYHF), CNPs or PP-CNPs for the association steps.

3.3. Cellular binding and uptake

To assess the cellular binding, 3×10^5 mGFP-CT26 cells were seeded into confocal dishes and incubated with PP-CNPs (0.067 μM based on PP) or PD-L1 Ab (0.067 μM) at 4 °C for 1 h. As a control experiments, mGFP-CT26 cells were pretreated with anti-PD-L1 antibody or peptide (PP; NYSKPTDRQYHF) at 4 °C for 1 h to block PD-L1 on the cell surface. The cellular uptake of PP-CNPs and PD-L1 Ab was investigated in mGFP-CT26 cells after treatment at 37 °C for 0, 1, 3, 6, 12 and 24 h. The lysosomes in the mGFP-CT26 cells were labeled by incubation with LAMP1-RFP fusion constructs (CellLight™ BacMam 2.0, Thermo Fisher Scientific, USA) for 1 h 37 °C. After treatment, cells were washed with DPBS for 2 min, fixed with 4% paraformaldehyde for 10 min, and stained with 4',6-diamidino-2-phenylindole (DAPI) for 5 min. Fluorescence imaging for cellular binding and uptake was performed by using a Leica TCS SP8 confocal laser-scanning microscope (CLSM; Leica Microsystems GmbH; Wetzlar, Germany). Quantitative analyses of the fluorescence images were performed using ImageJ software (NIH, Bethesda, MD, USA). For the analysis of PD-L1 expression, 1×10^6 CT26 cells were seeded in the 6-well cell culture plates. After 24 h of stabilization, the CT26 cells were incubated with PP-CNPs (0.067 μM based on PP), PP (0.067 μM) or PD-L1 Ab (0.067 μM) for 48 h. Then, the cells were solubilized by using RIPA buffer containing 1% protease inhibitors, and the resulting lysates were centrifuged at 14,000 rpm for 15 min to remove cell debris. 5 μg of proteins were resolved *via* sodium dodecyl sulfate-polyacrylamide gel electrophoresis (SDS-PAGE) on 12% gels and transferred to PVDF (polyvinylidene difluoride) membranes.

3.4. Co-culture study

Five-week-old male BALB/c mice were purchased from NaraBio (Pyeongtaek-si, Gyeonggi-do, Republic of Korea). Mice were bred under pathogen-free conditions at the Korea Institute of Science and Technology (KIST). All animal experiments were performed in compliance with the relevant laws and institutional guidelines of the Institutional Animal Care and Use Committee (IACUC; approval number KIST-IACUC-2023-013) of the Korea Institute of Science and Technology (KIST). The CD8$^+$ T cells were collected from the spleen and lymph nodes of BALB/c mice using a mouse CD8$^+$ T cell isolation kit and activated by using a T cell activation/expansion kit. Then, activated CD8$^+$ T cells were co-cultured with CT26 cells treated with PP-CNPs (0.067 μM based on PP) or PD-L1 Ab (0.067 μM) for 48 h. After 2 h of co-culture, photographs were captured using an optical microscope. In addition, IFN-γ in the co-culture medium was measured using an IFN-γ ELISA Kit. The tumor cell lysis by CD8$^+$ T cells was evaluated by

measuring viability of CT26 cells using the CCK-8 assay. For the analysis of CT26 cell viability, suspended T cells were washout with DPBS, and adherent CT26 cells were incubated with culture medium containing 10% CCK-8 solution. After 20 min of incubation, the cell viability was analyzed using a microplate reader (VERSAmaxTM; Molecular Devices Corp., USA) with a wavelength of 450 nm. To assess T cell proliferation after co-culture with CT26 cells treated with PP-CNPs or PD-L1 Ab, CD8$^+$ T cells were labeled with CFSE dye (Thermo Fisher Scientific Inc., Rockford, IL, USA), and the dilution assays were performed. Briefly, activated CD8$^+$ T cells were incubated with CFSE dye in serum-free culture medium at 37 °C for 5 min, and cells were resuspended in cell culture medium. After 2 h of co-culture with CT26 cells pre-treated with PP-CNPs or PD-L1 Ab, the decreased fluorescence intensities of daughter T cells was compared to parental cells after cell division owing to the dilution of CFSE dye.

3.5. In vivo tumor targeting of PP-CNPs and PD-L1 degradation

The tumor targeting and PD-L1 degradation of PP-CNPs were evaluated in CT26 tumor-bearing BALB/c mice that were prepared *via* subcutaneous inoculation of 1×10^6 CT26 cells. When the tumor volumes were approximately 200 mm^3, 10 mg/kg of Cy5.5-labeled PP-CNPs, CNPs, anti-PD-L1 Ab or peptide (PP; NYSKPTDRQYHF) were intravenously injected into mice. At the indicated time points, noninvasive near-infrared fluorescence (NIRF) imaging was performed *via* IVIS Lumina Series III system (PerkinElmer; Waltham, MA, USA). The tumor tissues were collected from the mice after 72 h of injection for *ex vivo* fluorescence imaging. The fluorescence intensities in tumor tissues were quantified using a Living Image software (PerkinElmer, Waltham, MA, USA). Finally, tumor tissues were cut into 10-μm thick sections for histological analyses. Slide-mounted tumor sections were stained with green fluorescent protein (GFP) fluorescent dye-conjugated anti-PD-L1 antibody for 6 h at 4 °C and analyzed using a Leica TCS SP8 confocal laser scanning microscope.

4. Cytotoxicity study

The cytotoxicity was assessed *via* the Cell Counting Kit-8 (CCK-8) assays. For these analyses, 3×10^5 CT26 cells or H9C2 rat cardiomyocytes were seeded into 96-well cell culture plates. Then, cells were treated with CNPs or PP-CNPs. After 48 h of incubation, the cells were incubated with cell culture medium containing 10% of CCK-8 solution for 15 min. The cell viability was analyzed using a microplate reader (VERSAmaxTM; Molecular Devices Corp., USA) with a wavelength of 450 nm. The cell viability of CT26 cells were also assessed after treatment with an equivalent DOX concentrations (1 μM) of free DOX, DOX-CNPs or DOX-PP-CNPs for 48 h.

4.1. DAMPs analysis

DAMP expressions from CT26 cells were analyzed by measuring CRT expression on cell surface and extracellular release of HMGB1. Briefly, 3 $\times 10^5$ CT26 cells were incubated with free DOX, DOX-CNPs or DOX-PP-CNPs (1 μM based on DOX content) at 37 °C for 48 h. Then, the cells were stained with APC-conjugated CRT antibody for 24 h at 4 °C and were subsequently washed with DPBS, fixed with 4% paraformaldehyde for 10 min, and stained with 4',6-diamidino-2-phenylindole (DAPI) for 5 min. Fluorescence imaging was performed by using a Leica TCS SP8 confocal laser scanning microscope. The CRT expression of CT26 cells was also assessed *via* flow cytometry after each treatment with same protocol (n = 3). Extracellular release of HMGB1 and ATP to the cell culture medium was measured using an ELISA assay kit and commercial ATP assay kit (Beyotime Biotechnology), respectively. The effective ICD effects by DOX-PP-CNPs were further evaluated through co-culture assays. For these analyses, 1×10^6 CT26 cells were seeded in 100-pi cell culture dishes, followed by treatment with PP-CNPs or an equivalent

DOX concentration (1 μM) of free DOX, DOX-CNPs or DOX-PP-CNPs for 48 h. In case of PP-CNPs, equal CNP amount with DOX-PP-CNPs was treated with CT26 cells. Then, CT26 cells were further co-cultured with lymphocytes from 6-week-old male BALB/C mice for 2 h, and the population of mature dendritic cells (CD11c$^+$CD40$^+$CD86$^+$) and activated T cells (CD45$^+$CD3$^+$CD8$^+$) within the lymphocytes was analyzed *via* flow cytometer (CytoFLEX, BECKMAN COULTER, USA).

4.2. Therapeutic efficacy and antitumor immune responses of PP-CNPs

The therapeutic efficacy was assessed in CT26 tumor-bearing mice. The 10 mg/kg of PD-L1 Ab, anti-PD-L1 peptide (PD-L1 pep; NYSKPTDRQYHF), CNPs or PP-CNPs was intravenously injected into mice once every three days. The therapeutic efficacy was evaluated by measuring the tumor volumes, calculated as the largest diameter x smallest diameter^2 x 0.53. The tumor volume was measured once every two days, and mice with a tumor size of 2000 mm^3 or higher were counted as dead. To analyze the antitumor immune responses after each treatment, the tumor tissues were collected on day 10. Single cells were isolated from the tumor tissues using a Tumor Dissociation Kit and incubated with FcBlock for 10 min to avoid non-specific antibody binding. Finally, multi-parameter staining was performed for 30 min to analyze the proportion of (i) cytotoxic T cells (CD45$^+$CD3$^+$CD8$^+$), (ii) regulatory T lymphocytes (Treg; CD45$^+$CD3$^+$CD4$^+$CD25$^+$), (iii) mature DCs (CD11c$^+$CD80$^+$) and (iv) PD-L1-positive tumor cells (CD45$^-$PD-L1$^+$), DCs (CD11c$^+$PD-L1$^+$) and macrophages (F4/80$^+$PD-L1$^+$) in the tumor tissues.

4.3. Therapeutic efficacy in lung metastasis model

To prepare lung metastasis mice models, 1×10^6 luciferase-expressing CT26 cells were intravenously injected into BALB/c mice. Five days after tumor inoculation, mice were treated with saline or equivalent doses (1 mg/kg based on DOX content) of free DOX, DOX-CNPs or DOX-PP-CNPs once every three days. At the pre-determined time points, noninvasive bioluminescence imaging was performed after intravenous injection of luciferin. For histological analysis, lung tissues from each group were collected on day 5 after treatment and stained with Alexa Fluor 647-conjugated anti-CD8 or anti-CD25 antibodies for 1 h at room temperature. Lung tissues were analyzed using a Leica TCS SP8 confocal laser scanning microscope.

4.4. Statistics

The statistical significance between two groups was analyzed using Student's t-test. One-way analysis of variance (ANOVA) was performed for comparisons of more than two groups, and multiple comparisons were analyzed using Tukey-Kramer post-hoc test. Survival data was plotted as Kaplan-Meier curves and analyzed using log-rank test. Statistical significance was indicated with asterisk (*p < 0.05, **p < 0.01, ***< 0.001) in the figures.

Ethics approval and consent to participate

Mice were bred under pathogen-free conditions at the Korea Institute of Science and Technology (KIST). All animal experiments were performed in compliance with the relevant laws and institutional guidelines of the Institutional Animal Care and Use Committee (IACUC; approval number 2023–013) of the Korea Institute of Science and Technology (KIST).

CRediT authorship contribution statement

Sukyung Song: Validation, Formal analysis, Investigation, Data curation, Visualization. **Man Kyu Shim:** Methodology, Formal analysis, Data curation, Writing – original draft. **Suah Yang:** Methodology,

Investigation. **Jaewan Lee:** Methodology. **Wan Su Yun:** Investigation. **Hanhee Cho:** Investigation. **Yujeong Moon:** Investigation. **Jin Young Min:** Investigation. **Eun Hee Han:** Methodology. **Hong Yeol Yoon:** Methodology. **Kwangmeyung Kim:** Conceptualization, Resources, Supervision, Funding acquisition, Project administration, Writing – original draft.

Declaration of competing interest

The authors declare that they have no known competing financial interests or personal relationships that could have appeared to influence the work reported in this paper.

Acknowledgements

Appendix A. Supplementary data

Supplementary data to this article can be found online at https://doi.org/10.1016/j.bioactmat.2023.05.016.

References

[1] J.R. Brahmer, S.S. Tykodi, L.Q.M. Chow, W.-J. Hwu, S.L. Topalian, P. Hwu, C.G. Drake, L.H. Camacho, J. Kauh, K. Odunsi, H.C. Pitot, O. Hamid, S. Bhatia, R. Martins, K. Eaton, S. Chen, T.M. Salay, S. Alaparthy, J.F. Grosso, A.J. Korman, S.M. Parker, S. Agrawal, S.M. Goldberg, D.M. Pardoll, A. Gupta, J.M. Wigginton, Safety and activity of anti–PD-L1 antibody in patients with advanced cancer, N. Engl. J. Med. 366 (26) (2012) 2455–2465.
[2] R.S. Herbst, J.-C. Soria, M. Kowanetz, G.D. Fine, O. Hamid, M.S. Gordon, J.A. Sosman, D.F. McDermott, J.D. Powderly, S.N. Gettinger, H.E.K. Kohrt, L. Horn, D.P. Lawrence, S. Rost, M. Leabman, Y. Xiao, A. Mokatrin, H. Koeppen, P.S. Hegde, I. Mellman, D.S. Chen, F.S. Hodi, Predictive correlates of response to the anti-PD-L1 antibody MPDL3280A in cancer patients, Nature 515 (7528) (2014) 563–567.
[3] M. Kyu Shim, S. Yang, I.-C. Sun, K. Kim, Tumor-activated carrier-free prodrug nanoparticles for targeted cancer Immunotherapy: preclinical evidence for safe and effective drug delivery, Adv. Drug Deliv. Rev. 183 (2022), 114177.
[4] W. Um, J. Park, H. Ko, S. Lim, H.Y. Yoon, M.K. Shim, S. Lee, Y.J. Ko, M.J. Kim, J.H. Park, D.-K. Lim, Y. Byun, I.C. Kwon, K. Kim, Visible light-induced apoptosis activatable nanoparticles of photosensitizer-DEVD-anticancer drug conjugate for targeted cancer therapy, Biomaterials 224 (2019), 119494.
[5] S. Yang, M.K. Shim, W.J. Kim, J. Choi, G.-H. Nam, J. Kim, J. Kim, Y. Moon, H.Y. Kim, J. Park, Y. Park, I.-S. Kim, J.H. Ryu, K. Kim, Cancer-activated doxorubicin prodrug nanoparticles induce preferential immune response with minimal doxorubicin-related toxicity, Biomaterials 272 (2021), 120791.
[6] Z. Li, H. Cai, Z. Li, L. Ren, X. Ma, H. Zhu, Q. Gong, H. Zhang, Z. Gu, K. Luo, A tumor cell membrane-coated self-amplified nanosystem as a nanovaccine to boost the therapeutic effect of anti-PD-L1 antibody, Bioact. Mater. 21 (2023) 299–312.
[7] R.M. Webster, The immune checkpoint inhibitors: where are we now? Nat. Rev. Drug Discov. 13 (12) (2014) 883–884.
[8] D.C. Binder, Y.-X. Fu, R.R. Weichselbaum, Radiotherapy and immune checkpoint blockade: potential interactions and future directions, Trends Mol. Med. 21 (8) (2015) 463–465.
[9] H. Wang, H. Yao, C. Li, H. Shi, J. Lan, Z. Li, Y. Zhang, L. Liang, J.-Y. Fang, J. Xu, HIP1R targets PD-L1 to lysosomal degradation to alter T cell–mediated cytotoxicity, Nat. Chem. Biol. 15 (1) (2019) 42–50.
[10] I. Visan, CMTM6 controls PD-L1, Nat. Immunol. 18 (10) (2017) 1067-1067.
[11] Y. Ren, Y. Qian, L. Ai, Y. Xie, Y. Gao, Z. Zhuang, J. Chen, Y.-X. Chen, J.-Y. Fang, TRAPPC4 regulates the intracellular trafficking of PD-L1 and antitumor immunity, Nat. Commun. 12 (1) (2021) 5405.
[12] M.L. Burr, C.E. Sparbier, Y.-C. Chan, J.C. Williamson, K. Woods, P.A. Beavis, E.Y. N. Lam, M.A. Henderson, C.C. Bell, S. Stolzenburg, O. Gilan, S. Bloor, T. Noori, D. W. Morgens, M.C. Bassik, P.J. Neeson, A. Behren, P.K. Darcy, S.-J. Dawson, I. Voskoboinik, J.A. Trapani, J. Cebon, P.J. Lehner, M.A. Dawson, CMTM6 maintains the expression of PD-L1 and regulates anti-tumour immunity, Nature 549 (7670) (2017) 101–105.
[13] P.R. Moody, E.J. Sayers, J.P. Magnusson, C. Alexander, P. Borri, P. Watson, A.T. Jones, Receptor crosslinking: a general method to trigger internalization and lysosomal targeting of therapeutic receptor:ligand complexes, Mol. Ther. 23 (12) (2015) 1888–1898.
[14] D.C. Radford, J. Yang, M.C. Doan, L. Li, A.S. Dixon, S.C. Owen, J. Kopeček, Multivalent HER2-binding polymer conjugates facilitate rapid endocytosis and enhance intracellular drug delivery, J. Contr. Release 319 (2020) 285–299.
[15] J. Bu, A. Nair, M. Iida, W.-j. Jeong, M.J. Poellmann, K. Mudd, L.J. Kubiatowicz, E.W. Liu, D.L. Wheeler, S. Hong, An avidity-based PD-L1 antagonist using nanoparticle-antibody conjugates for enhanced immunotherapy, Nano Lett. 20 (7) (2020) 4901–4909.
[16] M.K. Shim, J. Park, H.Y. Yoon, S. Lee, W. Um, J.-H. Kim, S.-W. Kang, J.-W. Seo, S.-W. Hyun, J.H. Park, Y. Byun, I.C. Kwon, K. Kim, Carrier-free nanoparticles of cathepsin B-cleavable peptide-conjugated doxorubicin prodrug for cancer targeting therapy, J. Contr. Release 294 (2019) 376–389.
[17] S. Lim, J. Park, M.K. Shim, W. Um, H.Y. Yoon, J.H. Ryu, D.K. Lim, K. Kim, Recent advances and challenges of repurposing nanoparticle-based drug delivery systems to enhance cancer immunotherapy, Theranostics 9 (25) (2019) 7906–7923.
[18] V. Torchilin, Tumor delivery of macromolecular drugs based on the EPR effect, Adv. Drug Deliv. Rev. 63 (3) (2011) 131–135.
[19] S. Yang, M.K. Shim, S. Song, H. Cho, J. Choi, S.I. Jeon, W.J. Kim, W. Um, J.H. Park, H.Y. Yoon, K. Kim, Liposome-mediated PD-L1 Multivalent Binding Promotes the Lysosomal Degradation of PD-L1 for T Cell-Mediated Antitumor Immunity, Biomaterials, 2022, 121841.
[20] J.H. Ryu, H.Y. Yoon, I.-C. Sun, I.C. Kwon, K. Kim, Tumor-targeting glycol chitosan nanoparticles for cancer heterogeneity, Adv. Mater. 32 (51) (2020), 2002197.
[21] J.H. Na, S.-Y. Lee, S. Lee, H. Koo, K.H. Min, S.Y. Jeong, S.H. Yuk, K. Kim, I.C. Kwon, Effect of the stability and deformability of self-assembled glycol chitosan nanoparticles on tumor-targeting efficiency, J. Contr. Release 163 (1) (2012) 2–9.
[22] D.-E. Lee, H. Koo, I.-C. Sun, J.H. Ryu, K. Kim, I.C. Kwon, Multifunctional nanoparticles for multimodal imaging and theragnosis, Chem. Soc. Rev. 41 (7) (2012) 2656–2672.
[23] J.Y. Yhee, S. Song, S.J. Lee, S.-G. Park, K.-S. Kim, M.G. Kim, S. Son, H. Koo, I.C. Kwon, J.H. Jeong, Cancer-targeted MDR-1 siRNA delivery using self-cross-linked glycol chitosan nanoparticles to overcome drug resistance, J. Contr. Release 198 (2015) 1–9.
[24] K. Park, J.-H. Kim, Y.S. Nam, S. Lee, H.Y. Nam, K. Kim, J.H. Park, I.-S. Kim, K. Choi, S.Y. Kim, I.C. Kwon, Effect of polymer molecular weight on the tumor targeting characteristics of self-assembled glycol chitosan nanoparticles, J. Contr. Release 122 (3) (2007) 305–314.
[25] J.H. Na, H. Koo, S. Lee, K.H. Min, K. Park, H. Yoo, S.H. Lee, J.H. Park, I.C. Kwon, S.Y. Jeong, K. Kim, Real-time and non-invasive optical imaging of tumor-targeting glycol chitosan nanoparticles in various tumor models, Biomaterials 32 (22) (2011) 5252–5261.
[26] S. Lee, S.-W. Kang, J.H. Ryu, J.H. Na, D.-E. Lee, S.J. Han, C.M. Kang, Y.S. Choe, K. C. Lee, J.F. Leary, K. Choi, K.-H. Lee, K. Kim, Tumor-Homing glycol chitosan-based optical/PET dual imaging nanoprobe for cancer diagnosis, Bioconjugate Chem. 25 (3) (2014) 601–610.
[27] S. Wilhelm, A.J. Tavares, Q. Dai, S. Ohta, J. Audet, H.F. Dvorak, W.C.W. Chan, Analysis of nanoparticle delivery to tumours, Nat. Rev. Mater. 1 (5) (2016), 16014.
[28] H. Koo, M.S. Huh, I.-C. Sun, S.H. Yuk, K. Choi, K. Kim, I.C. Kwon, In vivo targeted delivery of nanoparticles for theranosis, Acc. Chem. Res. 44 (10) (2011) 1018–1028.
[29] Y. Choi, H. Han, S. Jeon, H.Y. Yoon, H. Kim, I.C. Kwon, K. Kim, Deep tumor penetration of doxorubicin-loaded glycol chitosan nanoparticles using high-intensity focused ultrasound, Pharmaceutics 12 (10) (2020).
[30] K. Kim, J.H. Kim, H. Park, Y.-S. Kim, K. Park, H. Nam, S. Lee, J.H. Park, R.-W. Park, I.-S. Kim, K. Choi, S.Y. Kim, K. Park, I.C. Kwon, Tumor-homing multifunctional nanoparticles for cancer theragnosis: simultaneous diagnosis, drug delivery, and therapeutic monitoring, J. Contr. Release 146 (2) (2010) 219–227.
[31] H.-Y. Hwang, I.-S. Kim, I.C. Kwon, Y.-H. Kim, Tumor targetability and antitumor effect of docetaxel-loaded hydrophobically modified glycol chitosan nanoparticles, J. Contr. Release 128 (1) (2008) 23–31.
[32] J.-H. Kim, Y.-S. Kim, K. Park, S. Lee, H.Y. Nam, K.H. Min, H.G. Jo, J.H. Park, K. Choi, S.Y. Jeong, R.-W. Park, I.-S. Kim, K. Kim, I.C. Kwon, Antitumor efficacy of cisplatin-loaded glycol chitosan nanoparticles in tumor-bearing mice, J. Contr. Release 127 (1) (2008) 41–49.
[33] K.H. Min, K. Park, Y.-S. Kim, S.M. Bae, S. Lee, H.G. Jo, R.-W. Park, I.-S. Kim, S.Y. Jeong, K. Kim, I.C. Kwon, Hydrophobically modified glycol chitosan nanoparticles-encapsulated camptothecin enhance the drug stability and tumor targeting in cancer therapy, J. Contr. Release 127 (3) (2008) 208–218.
[34] S.J. Lee, H. Koo, H. Jeong, M.S. Huh, Y. Choi, S.Y. Jeong, Y. Byun, K. Choi, K. Kim, I.C. Kwon, Comparative study of photosensitizer loaded and conjugated glycol chitosan nanoparticles for cancer therapy, J. Contr. Release 152 (1) (2011) 21–29.
[35] S.J. Lee, K. Park, Y.-K. Oh, S.-H. Kwon, S. Her, I.-S. Kim, K. Choi, S.J. Lee, H. Kim, S.G. Lee, K. Kim, I.C. Kwon, Tumor specificity and therapeutic efficacy of photosensitizer-encapsulated glycol chitosan-based nanoparticles in tumor-bearing mice, Biomaterials 30 (15) (2009) 2929–2939.
[36] C.K. Lee, D.F. Atibalentja, L.E. Yao, J. Park, S. Kuruvilla, D.W. Felsher, Anti-PD-L1 f (ab) conjugated PEG-PLGA nanoparticle enhances immune checkpoint therapy, Nanotheranostics 6 (3) (2022) 243.
[37] S. Xu, F. Cui, D. Huang, D. Zhang, A. Zhu, X. Sun, Y. Cao, S. Ding, Y. Wang, E. Gao, PD-L1 monoclonal antibody-conjugated nanoparticles enhance drug delivery level and chemotherapy efficacy in gastric cancer cells, Int. J. Nanomed. 14 (2019) 17.
[38] Y. Yu, J. Li, B. Song, Z. Ma, Y. Zhang, H. Sun, X. Wei, Y. Bai, X. Lu, P. Zhang, Polymeric PD-L1 blockade nanoparticles for cancer photothermal-immunotherapy, Biomaterials 280 (2022), 121312.
[39] M.K. Shim, H.Y. Yoon, J.H. Ryu, H. Koo, S. Lee, J.H. Park, J.H. Kim, S. Lee, M.G. Pomper, I.C. Kwon, Cathepsin B-specific metabolic precursor for in vivo tumor-specific fluorescence imaging, Angew. Chem. 128 (47) (2016) 14918–14923.

[40] J.E. Moses, A.D. Moorhouse, The growing applications of click chemistry, Chem. Soc. Rev. 36 (8) (2007) 1249–1262.

[41] H.C. Kolb, K.B. Sharpless, The growing impact of click chemistry on drug discovery, Drug Discov. Today 8 (24) (2003) 1128–1137.

[42] J. Fang, H. Nakamura, H. Maeda, The EPR effect: unique features of tumor blood vessels for drug delivery, factors involved, and limitations and augmentation of the effect, Adv. Drug Deliv. Rev. 63 (3) (2011) 136–151.

[43] H. Li, J. Sun, H. Zhu, H. Wu, H. Zhang, Z. Gu, K. Luo, Recent advances in development of dendritic polymer-based nanomedicines for cancer diagnosis, Wiley Interdisciplinary Reviews: Nanomedicine and Nanobiotechnology 13 (2) (2021), e1670.

[44] J.W. Kleinovink, K.A. Marijt, M.J.A. Schoonderwoerd, T. van Hall, F. Ossendorp, M.F. Fransen, PD-L1 expression on malignant cells is no prerequisite for checkpoint therapy, OncoImmunology 6 (4) (2017), e1294299.

[45] H. Liu, X. Bi, Y. Zhou, R. Shi, S. Yao, J. Qi, H. Feng, M. Feng, J. Yan, S. Tan, Identification of a hotspot on PD-L1 for pH-dependent binding by monoclonal antibodies for tumor therapy, Signal Transduct. Targeted Ther. 5 (1) (2020) 158.

[46] J. Qin, M. Zhang, Y. Guan, X. Guo, Z. Li, C. Rankl, J. Tang, Imaging and quantifying analysis the binding behavior of PD-L1 at molecular resolution by atomic force microscopy, Anal. Chim. Acta 1191 (2022), 339281.

[47] G.A. Eggimann, S. Buschor, T. Darbre, J.-L. Reymond, Convergent synthesis and cellular uptake of multivalent cell penetrating peptides derived from Tat, Antp, pVEC, TP10 and SAP, Org. Biomol. Chem. 11 (39) (2013) 6717–6733.

[48] L. Li, Y. Li, C.-H. Yang, D.C. Radford, J. Wang, M. Janát-Amsbury, J. Kopeček, J. Yang, Inhibition of immunosuppressive tumors by polymer-assisted inductions of immunogenic cell death and multivalent PD-L1 crosslinking, Adv. Funct. Mater. 30 (12) (2020), 1908961.

[49] R. Zaman, R.A. Islam, N. Ibnat, I. Othman, A. Zaini, C.Y. Lee, E.H. Chowdhury, Current strategies in extending half-lives of therapeutic proteins, J. Contr. Release 301 (2019) 176–189.

[50] S.A. Oh, D.-C. Wu, J. Cheung, A. Navarro, H. Xiong, R. Cubas, K. Totpal, H. Chiu, Y. Wu, L. Comps-Agrar, PD-L1 expression by dendritic cells is a key regulator of T-cell immunity in cancer, Nat. Can. (Que.) 1 (7) (2020) 681–691.

[51] H.Y. Yoon, S. Son, S.J. Lee, D.G. You, J.Y. Yhee, J.H. Park, M. Swierczewska, S. Lee, I.C. Kwon, S.H. Kim, Glycol chitosan nanoparticles as specialized cancer therapeutic vehicles: sequential delivery of doxorubicin and Bcl-2 siRNA, Sci. Rep. 4 (1) (2014) 1–12.

[52] H.Y. Nam, S.M. Kwon, H. Chung, S.-Y. Lee, S.-H. Kwon, H. Jeon, Y. Kim, J.H. Park, J. Kim, S. Her, Cellular uptake mechanism and intracellular fate of hydrophobically modified glycol chitosan nanoparticles, J. Contr. Release 135 (3) (2009) 259–267.